Published in final edited form as:
Biochemistry. 2008 August 26; 47(34): 9016–9028. doi:10.1021/bi800486x.

The transcription regulator RcoM-2 from *Burkholderia xenovorans* is a cysteine-ligated hemoprotein that undergoes a redox-mediated ligand switch

Katherine A. Marvin[1], **Robert L. Kerby**[2], **Hwan Youn**[2], **Gary P. Roberts**[2], and **Judith N. Burstyn**[1,*]

[1]Department of Chemistry, University of Wisconsin-Madison, 1101 University Ave. Madison, WI, 53706

[2]Department of Bacteriology, University of Wisconsin-Madison, 1550 Linden Dr. Madison, WI, 53706

Abstract

Spectroscopic characterization of the newly discovered heme-PAS domain sensor protein *Bx*RcoM-2 reveals that this protein undergoes redox-dependent ligand switching and CO- and NO-induced ligand displacement. The aerobic bacterium *Burkholderia xenovorans* expresses two homologous heme-containing proteins that promote CO-dependent transcription *in vivo*. These regulators of CO metabolism, *Bx*RcoM-1 and *Bx*RcoM-2, are gas-responsive heme-PAS domain proteins like the mammalian neuronal PAS domain protein 2 (NPAS2) and the direct oxygen sensor from *E. coli* (*Ec*Dos). *Bx*RcoM-2 was studied using electronic absorption, MCD, resonance Raman and EPR spectroscopies. In the Fe(III) oxidation state, the heme is low-spin and 6-coordinate with a cysteine (thiolate) as one of the two ligands. The sixth ligand is a histidine (His^{74}), which is present in all states of the protein studied. Reduction to the Fe(II) oxidation state results in replacement of the cysteine(thiolate) by a neutral thioether ligand, Met^{104}. CO and NO bind to the Fe(II)*Bx*RcoM-2 heme opposite the histidine ligand. Thus, *Bx*RcoM-2 employs similar coordination state changes to those known for CO-sensing CooA, with redox dependent loss of a cysteine(thiolate) ligand and displacement of a relatively weakly bound axial ligand by the effector gas molecule. Like *Ec*Dos, the weakly bound axial ligand that is displaced is methionine.

The past decade has witnessed the discovery of many new heme-containing gas-sensing proteins, which couple the binding of diatomic ligands at a heme center to the regulation of protein function. Binding of O_2, CO, or NO effector molecules to heme iron acts as a switch for an allosteric conformational change; the environment of the heme pocket often discriminates against functional activation by more than one specific ligand (1,2). Oxygen sensors include bacterial FixL (3), *Ec*Dos (4), and HemAT (5); the CO sensors include bacterial *Rr*CooA (6) and mammalian NPAS2 (7); and the NO sensors include mammalian sGC (8) and bacterial H-NOX proteins (9). This diverse collection of proteins frequently utilizes a single-component signal transduction system with a heme-binding domain and a functional domain, which may be a guanylyl cyclase, phosphodiesterase, or DNA binding domain. We report

*To whom all correspondence should be addressed Tel: 608−262−0328 Fax: 608−262−6143 E-mail: burstyn@chem.wisc.edu.

†This work was supported by N.I.H. grants HL-66147 (J.N.B.) and GM-53228 (G.P.R.)

SUPPORTING INFORMATION AVAILABLE

Figures showing the MCD spectrum of Fe(III)RcoM-2 (S1), the rR spectrum of Fe(II)-NO RcoM-2 (S3), and correlation plots of ν(Fe-CO) versus ν(C-O) (S2) and ν(Fe-NO) versus ν(N-O) (S4). Parameters used to fit the EPR spectrum of Figure 2. Tables supporting the spectral interpretation S1-S6. This material is available free of charge via the Internet at http://pubs.acs.org.

herein spectroscopic characterization of a new protein of this class, *Bx*RcoM-2, a putative regulator of aerobic CO metabolism.

A number of heme-based sensor proteins, including FixL, *Ec*Dos and NPAS2, bind heme within a conserved PAS domain. PAS domains are found in proteins spanning all kingdoms of life (10). The basic domain structure is an α/β fold of ~130 aa, although the sequence identity among PAS-bearing proteins is quite low. Sensing environmental signals through small molecule binding is a function associated with PAS domains. Only a few PAS-containing proteins are known to bind cofactors such as FAD, FMN and heme, and among these the heme-containing PAS domain proteins are the best-characterized. The heme-PAS sensor kinase FixL is the regulator of a two-component signal transduction system, which phosphorylates the transcription factor FixJ (3,11). Under aerobic conditions, binding of O_2 to the heme in FixL inhibits kinase activity. Release of O_2 from the heme under hypoxic conditions stimulates phosphorylation of FixJ, triggering a cascade that results in production of the nitrogen fixation machinery. CO and NO also inhibit the kinase activity of FixL, although with much reduced efficiency (3- and 2-fold for CO and NO, respectively, versus 100-fold for O_2) (12,13).

The direct oxygen sensor in *E. coli* (*Ec*Dos) (4) and the *Acetobacter xylinum* phosphodiesterase A1 (*Ax*PDEA1) (14) proteins are closely related to one another and to FixL, with PAS-domains whose sequences are ~30% identical to that of FixL. These proteins combine a N-terminal PAS-fold heme domain with a phosphodiesterase enzymatic domain, a module found only in bacterial signal transduction systems. *Ax*PDEA1 regulates cellulose synthase, which is allosterically activated by the precursor molecule 3', 5'-cyclic diguanylic acid (c-di-GMP). Under aerobic conditions *Ax*PDEA1 is inhibited by O_2 binding to the PAS-domain heme. As oxygen tension decreases and O_2 is released, phosphodiesterase activity is stimulated, hydrolyzing c-di-GMP to the linear dinucleotide (pGpG) and inhibiting cellulose production. *Ec*Dos shares approximately 40% sequence identity with *Ax*PDEA1 over the heme and enzymatic domains (4). *Ec*Dos exhibits O_2-dependent cAMP phosphodiesterase activity (15), as well as O_2-, CO- and NO-dependent c-di-GMP phosphodiesterase activity (16). Spectroscopic, structural and mutagenesis studies indicate that *Ec*Dos is low-spin and 6-coordinate in the Fe(III), Fe(II), and Fe(II) gas-bound states, and that signal transduction occurs via displacement of an endogenous ligand (Met^{95}) (15-17).

PAS-domain heme-based sensor proteins are also known to bind to DNA and to function as transcriptional regulators. The neuronal PAS domain protein 2 (NPAS2) was the first eukaryotic heme-containing PAS-domain protein identified (7). NPAS2 is a transcription factor that binds to DNA as a heterodimer with BMAL1. NPAS2 is expressed in the central nervous system, where it regulates the expression of genes critical to controlling circadian rhythm (18). Each of the two PAS domains in NPAS2 contains a heme, and the binding of CO inhibits heterodimerization with BMAL1 and thus prevents transcription of NPAS2-BMAL1 regulated target genes (7).

CooA (CO oxidation activator) is a CO sensor from the bacterium *Rhodospirillum rubrum* and is the most throroughly characterized heme-based sensor protein (6,19). *Rr*CooA, which does not contain a PAS domain, is a member of the cAMP receptor protein (CRP) and fumarate and nitrate reductase (FNR) superfamily of transcriptional regulators. In the absence of oxygen, the specific binding of CO to the *Rr*CooA heme activates transcription of the genes for the CO-oxidation machinery, thus enabling *R. rubrum* to utilize CO as an energy source. The *Rr*CooA homodimer consists of two domains: a N-terminal heme-binding regulatory domain and a C-terminal helix-turn-helix DNA-binding domain (20). The *Rr*CooA dimer binds two *b*-type heme cofactors in each regulatory domain; the Fe(III) heme iron is coordinated by cysteine (thiolate) (Cys^{75}) and by the nitrogen of the opposing monomer's N-terminal proline (Pro^{2}) (21). When the heme is reduced, the cysteine(thiolate) is replaced by a neighboring histidine

(His^{77}) (22,23), which poises the protein to bind CO via replacement of the coordinated proline. The binding of CO is proposed to trigger a global conformational change in which movement of the heme is translated through the dimer interface to the DNA binding domain (24,25).

The newest members of the heme-based sensor family are heme-PAS transcription factors that may regulate aerobic CO metabolism in bacteria. Two proteins were isolated from *Burkholderia xenovorans* (LB400) (26), an aerobic polychlorinated biphenyl (PCB)-degrading bacterium originally found in PCB contaminated landfill sites in New York State (27). Designated "Regulators of CO Metabolism" (RcoM), these two homologous proteins (*Bx*RcoM-1 and *Bx*RcoM-2, 88% sequence identity, 93% sequence similarity) function as CO-dependent transcription factors *in vivo* (26). Each protein contains a N-terminal heme-containing PAS domain and a C-terminal LytTR DNA binding domain. The N-terminal PAS domain binds a *b*-type heme, and mutagenesis of two conserved residues, His^{74} and Met*104* in *Bx*RcoM-1, identified these residues as likely heme iron axial ligands.

Herein, we describe the spectroscopic characterization of the *Bx*RcoM-2 protein in the Fe(III), Fe(II), Fe(II)CO and Fe(II)NO states using the techniques of electronic absorption, magnetic circular dichroism, electron paramagnetic resonance and resonance Raman spectroscopy. Our studies reveal that one of the two axial ligands in Fe(III)*Bx*RcoM-2 is a cysteine(thiolate) that is replaced by a neighboring neutral residue, likely Met^{104}, upon reduction of the heme iron. Binding of CO to the Fe(II) heme occurs opposite a neutral endogenous donor, likely His^{74}, while NO binds with retention of a sixth nitrogen-containing ligand, presumably the same histidine. Drawing on our spectroscopic data, previous mutational analysis and comparison to similar heme-containing PAS domain proteins (26), we propose a model for heme coordination changes in *Bx*RcoM-2 that are associated with redox and ligand binding events.

MATERIALS AND METHODS

Materials

CO and NO gas (99.5%) cylinders were purchased from AGA, and ^{13}CO gas (99%) was purchased from Sigma-Aldrich. The NO gas was passed over an anaerobic KOH column to remove higher order nitrogen oxides before use. Na^{15}NO$_2$ (98%) was purchased from Cambridge Isotopes, while NaNO$_2$ was purchased from Fischer Scientific. Buffer and glycerol and were purchased from Sigma-Aldrich; high purity sodium dithionite was purchased from Fluka and stored under Ar$_{(g)}$ at −20 °C. All chemical reagents were used as received.

Expression and purification of B*x*RcoM-2

The cloning, expression and purification of the *Bx*RcoM proteins has been described (26). In brief, the ~800 bp region encoding *Bx*RcoM-2 was cloned into pEXT20 (28) with subsequent introduction of a segment that added a 6-His tag at the C-terminus of the expressed protein. For expression, *E. coli* cultures were grown in rich medium supplemented with ferric citrate and IPTG, and the protein was purified as previously described (26). The purified protein was desalted by gel filtration into 25 mM MOPS pH 7.4 / 500 mM KCl, and stored at −80°C. Protein concentration was determined using the BCA method (Pierce, Rockford IL) using bovine serum albumin as the standard, and heme content was determined using the pyridine hemochrome assay (29). Protein purity was >90% by SDS-PAGE analysis.

Electronic Absorption Spectroscopy

Electronic absorption spectra were recorded on a double-beam Varian Cary 4 Bio spectrophotometer equipped with a temperature controller and set to a spectral bandwidth of 0.5 nm. Spectra were obtained at 25 °C for protein samples diluted into 25 mM EPPS and 500 mM KCl, pH 8.0. Protein solutions were purged with Ar$_{(g)}$ in the cuvette headspace to remove

O_2. Reactions of the Fe(III) protein with a reducing agent (sodium dithionite, $Na_2S_2O_4$) were performed anaerobically and were initiated by: 1) the addition of an excess of the solid reductant under $Ar_{(g)}$, or 2) the addition of a stock solution of reductant, prepared anaerobically, to a final concentration of 2 mM. The specific method used is noted in individual figure legends. The Fe(II)CO adducts of *Bx*RcoM-2 were generated by injection of $CO_{(g)}$ into the headspace of the septum-sealed cuvette via gastight syringe, after which the solution was gently agitated. $CO_{(g)}$ was introduced either to the Fe(III) protein, followed by reduction, or to the pre-reduced Fe(II) protein to observe any order of addition effects. The Fe(II)NO adducts of *Bx*RcoM-2 were generated by injection of $NO_{(g)}$ into the headspace of the septum-sealed cuvette via gastight syringe, after which the solution of Fe(III)*Bx*RcoM-2 or dithionite-reduced Fe(II) *Bx*RcoM-2 was gently agitated. Typically, 50−200 μL of $NO_{(g)}$ or $CO_{(g)}$ was used to form the NO and CO adducts; absorption spectra were recorded during the experiment at room temperature until no further changes were observed.

MCD Spectroscopy

Magnetic circular dichroism (MCD) spectra were recorded on a Jasco J-715 CD spectropolarimeter with the sample compartment modified to accommodate an Oxford Instruments SM-4000−8T magnetocryostat. MCD spectra were taken at temperatures ranging from 2 to 100 K. The MCD signal at −7 T for each temperature was subtracted from the +7 T data, and the resulting trace was divided by 2 to remove the CD contribution to each spectrum. The buffer used for MCD samples was 50 mM EPPS, 500 mM KCl, pH 8.0, with approximately 55% v/v glycerol present in the sample. Addition of glycerol had no effect on the visible absorption spectrum of any sample at room temperature, nor was any visible spectral change observed at temperatures at which MCD data were collected. Sodium dithionite was used as a reducing agent and was introduced in excess as a solid into anaerobic samples of the Fe(III) protein under $Ar_{(g)}$. CO and NO adducts were prepared as noted for the absorption spectra. Each sample was transferred to an $Ar_{(g)}$-filled cell via gastight syringe and frozen in liquid nitrogen.

EPR Spectroscopy

X-band EPR spectra were collected on a Bruker ESP 300E equipped with an Oxford ESR 900 continuous flow liquid helium cryostat and an Oxford ITC4 temperature controller. The microwave frequency was monitored using an EIP model 625A CW microwave frequency counter. Spectra were obtained at 10 K. Spectra of Fe(III) and Fe(II)NO *Bx*RcoM-2 (150 μL, ~250 μM heme) were recorded in 50 mM borate ($B(OH)_3$)) buffer with an additional 500mM KCl at pH 8.0. For samples containing reducing agent, sodium dithionite was added as a solid into anaerobic samples of the Fe(III) protein. The NO gas adducts were prepared using $Na^{14}NO_2$ or $Na^{15}NO_2$; NO gas was generated under anaerobic conditions *in situ* by the reduction of the appropriate $NaNO_2$ reagent with a small excess of sodium dithionite in the aqueous protein solution. Each sample was then transferred to an $Ar_{(g)}$-filled quartz EPR tube via gastight syringe or $Ar_{(g)}$-purged small-bore tubing and frozen in liquid nitrogen. For all samples, scans of 0−10,000 G revealed no signals other than those reported. EPR data were simulated using the WEPR program written by Dr. Frank Neese (30). The parameter set employed for the EPR simulation is given in the Supporting Information.

Resonance Raman Spectroscopy

Resonance Raman spectra were obtained with an excitation wavelength of 413.1 and 406.7 nm from a Kr^+ laser (Coherent I-302C). The scattered light was collected using a backscattering 135° sample geometry. Low incident laser powers of ~50 mW for Fe(III) and Fe(II) states, or ~7−10 mW for CO and NO adducts to minimize photodissociation of ligands, were focused with a cylindrical lens onto the sample. An Acton Research triple monochromator equipped

with 2400 grooves/mm gratings was used. Data were collected with a Princeton Instruments Spex 1877 triple spectrograph equipped with a cooled, intensified diode array detector. Data collection was automated using Spectrasense software. Peak positions and intensities were calibrated using the ice peak at 228 cm^{-1}. The frozen protein samples, in the same buffer as used for EPR (*vide infra*), were placed in a quartz dewar and cooled to 77 K to reduce local heating. Windows centered at 650, 1250 and 1850 cm^{-1} were collected to obtain a complete spectral window of ~150−2250 cm^{-1}. All spectral data were imported to and processed with IGOR Pro software (Wavemetrics, Inc.). Vibrational modes are indicated in the figures, with assignments based on comparison with those of other heme proteins and the work of Spiro and Kitagawa (31-34).

RESULTS

*Characterization of Fe(III)*B*x*RcoM-2*

The electronic absorption spectrum of Fe(III)*Bx*RcoM-2 (Figure 1) shows optical features with close similarities to those of known Fe(III) heme-thiolate proteins. The spectrum shown in Figure 1 is consistent with a low-spin, 6-coordinate Fe(III) heme with an axial ligand environment consisting of a cysteine(thiolate) ligand opposite a neutral donor ligand, likely histidine. Key spectral characteristics are a δ band at 354 nm, an intense Soret (γ) peak at 423 nm and broad, asymmetric α-β features at 565 and 541 nm, respectively, and a pair of weak charge transfer bands at ~640 and 730 nm. The two most significant optical features associated with coordination by cysteine(thiolate) include the δ band in the near-UV and charge-transfer bands in the visible region (35). The δ band is a feature associated with mixing of a sulfur-based ligand-to-metal charge transfer (LMCT) transition and the Fe(III) porphyrin($\pi \rightarrow \pi^*$) Soret transition. Additionally, when an Fe(III) heme is coordinated by a strong electron donor such as thiolate, the absorption spectrum exhibits two low-energy LMCT bands. Comparison of the spectral peak positions observed in Fe(III)*Bx*RcoM-2 (Table 1) with other known heme-thiolate proteins such as CooA from *R. rubrum*, cytochrome P450 with imidazole and human cystathione β-synthase (hCBS) provides support for the assignment of Fe(III)*Bx*RcoM-2 as another member of the class of 6-coordinate, low-spin heme-thiolate proteins.

The assignment of the Fe(III)*Bx*RcoM-2 as low-spin and 6-coordinate is also supported by the MCD spectral features. The MCD spectrum of Fe(III)*Bx*RcoM-2 shown in Supporting Information Figure S1 is dominated by an intense temperature-dependent, derivative-shaped *C*-term in the Soret region with a crossover at 419 nm. Another temperature-dependent *C*-term is also present in the α-β region with a crossover at 570 nm; the intensity of this term is much less than that of the Soret feature. A magnetization plot (Δε vs. βH/2kT) of data for Fe(III) *Bx*RcoM-2 (Supporting Information Figure S1, inset) is consistent with a low-spin, $S = 1/2$ heme . Comparison of the MCD peak positions of Fe(III)*Bx*RcoM-2 (Supporting Information Table S1) to other low-spin, 6-coordinate Fe(III) heme proteins is consistent with the assignment of axial ligation by cysteine(thiolate) opposite a neutral donor such as histidine.

EPR, which is sensitive to the unpaired spin density on iron and the axial ligand environment, is clearly indicative of cysteine(thiolate) ligated to the Fe(III)*Bx*RcoM-2 heme in a low-spin, 6-coordinate system. The corrected and simulated spectra for Fe(III)*Bx*RcoM-2 at pH 8.0 are depicted in Figure 2. The best-fit simulation yields *g* values of 1.88, 2.28 and 2.52 for $g_{x,}$ g_y and g_z, respectively. Table 2 illustrates that these values are in agreement with those of other Fe(III) heme proteins bearing cysteine(thiolate) coordinated opposite a neutral sixth ligand. A second, minor EPR signal with a narrower *g* anisotropy is observed in Fe(III)*Bx*RcoM-2 (Figure 2); this signal was not simulated due to the very low intensity and the extent of overlap with the major signal. The presence of dual signals in low-spin heme-thiolate proteins, which may be due to differences in protonation of the thiolate ligand (36), has been observed for both *Rr*CooA(37) and hCBS (38). The *g* anisotropy in low-spin Fe(III) hemes correlates with the

nature of the axial ligands and the narrow separation of g_x, g_y, and g_z provides definitive evidence for a thiolate ligand in Fe(III)*Bx*RcoM-2 (Table 2 and references therein) (39). In contrast, low-spin, Fe(III) heme proteins bearing two neutral donors (i.e. bis-histidine) typically exhibit a rhombic spectrum in which the *g* anisotropy is larger, e.g. cytochrome b_5 and neuroglobin. In cases where the axial ligands impose higher symmetry on the d_{xz} and d_{yz} iron orbitals, e.g. in *Ec*Dos, the unpaired electron becomes significantly delocalized, moving g_z (g_{max}) to lower field while g_x and g_y become broad and nearly undetectable. Blumberg and Peisach (39) utilized the energy parameters *V* and Δ as indicators of the strength and symmetry of the ligand field exerted by the axial ligands in low-spin Fe(III) hemes. Their analysis defined five regions in a crystal field diagram, which plotted the rhombic field (V/Δ) versus the tetragonal field (Δ/λ). Calculations using the *g* values measured for Fe(III)*Bx*RcoM-2 yield field parameters that place *Bx*RcoM-2 squarely within the 'P' region of the Blumberg-Peisach diagram, which is populated by other cysteine(thiolate) Fe(III) heme proteins possessing a sixth neutral axial ligand.

Resonance Raman analysis of Fe(III)*Bx*RcoM-2 (Figure 3B) identified vibrational modes associated with oxidation, spin and coordination states that are also consistent with a low-spin, 6-coordinate Fe(III) heme. The high frequency region of heme Raman spectra is dominated by porphyrin in-plane modes, which are sensitive to the heme iron oxidation state (ν_4) and spin and coordination states (ν_3, ν_2 and ν_{10}) (33, 34). The Soret-excited resonance Raman spectrum for Fe(III)*Bx*RcoM-2, shown in Figure 3B, displays porphyrin skeletal modes at frequencies expected for a low-spin Fe(III) heme: 1371 cm^{-1} (ν_4), 1500 cm^{-1} (ν_3), 1579 cm^{-1} (ν_4) and 1634 cm^{-1} (ν_{10}). Fe(III) heme centers exhibit the oxidation state marker band ν_4 in the range ~1370−1375 cm^{-1}, and for low-spin hemes the most distinct spin state marker band ν_3 occurs in the range of 1500−1510 cm^{-1} (33, 34). In contrast, high-spin, 5- and 6-coordinate Fe(III) hemes exhibit ν_3 at 1490−1500 cm^{-1} and 1475−1485 cm^{-1}, respectively. Though the porphyrin skeletal modes are largely insensitive to the identity of the iron axial ligands, the low-frequency region (200−700 cm^{-1}) can be useful in assigning vibrations associated with specific metal-ligand bonds (40). In previous work, Champion, *et al.* (41) characterized substrate-bound cytochrome $P450_{CAM}$ isotopically labeled with ^{34}S and ^{57}Fe and identified the stretching mode for the iron-sulfur bond ($\nu_{Fe\text{-}S}$ at 351 cm^{-1} for the high-spin Fe(III) enzyme. In the 6-coordinate, low-spin Fe(III) heme of hCBS, global ^{34}S labeling was used to identify ($\nu_{Fe\text{-}S}$ as a lower-energy band at 312 cm^{-1} (42). In Figure 3A, by analogy to the assignment in hCBS, we tentatively identify $\nu_{Fe\text{-}S}$ as a broad band centered at ~310 cm^{-1}; however definitive assignment of this mode cannot be made without isotopic labelling. The breadth of this ~310 cm^{-1} band suggests that there may be overlap of two different bond vibrations or slightly different environments around the thiolate ligand.

*Characterization of Fe(II)*Bx*RcoM-2*

Treatment of Fe(III)*Bx*RcoM-2 with a reducing agent results in a new electronic absorption spectrum suggestive of a low-spin, 6-coordinate Fe(II) heme in which the cysteine(thiolate) ligand has been replaced. As shown in Figure 4A, when reductant is added to Fe(III)*Bx*RcoM-2 the Soret band maximum increases in intensity and red shifts slightly from 423 nm to 425 nm with simultaneous sharpening of the α-β peaks, which shift to 562 and 532 nm, respectively (Figure 4A). Comparison of the spectral peak positions for Fe(II)*Bx*RcoM-2 (Table 3 and references therein) with those of other heme proteins such as *Rr*CooA, which undergo a ligand switch upon reduction, strongly suggests analogous behavior for *Bx*RcoM-2. If cysteine (thiolate) were retained as an axial ligand after reduction of Fe(III)*Bx*RcoM-2, the Soret maximum would be expected to appear at ~450 nm, as seen in reduced hCBS at pH 9. This is clearly not the case: the Soret maximum of Fe(II)*Bx*RcoM-2 at 425 nm in Figure 4A shows conclusively that cysteine(thiolate) is replaced as an axial ligand. In the case of Fe(II)CooA, cysteine(thiolate) is replaced by a histidine; this change in coordination results in a Soret

maximum with an identical peak position to Fe(II)*Bx*RcoM-2 (425 nm), though the α-β positions of Fe(II)CooA are both blue-shifted 3 nm relative to those of Fe(II)*Bx*RcoM-2. Cytochrome b_5 and neuroglobin, which possess bis-histidine coordination in the Fe(II) state, also display similar Soret positions to those of Fe(II)*Bx*RcoM-2 and Fe(II)CooA (Table 3), supporting an assignment in Fe(II)*Bx*RcoM-2 of two neutral donor axial ligands. When α-β peak positions are considered, the observed spectral data for Fe(II)*Bx*RcoM-2 most closely resemble those of Fe(II)*Ec*Dos (4), which possesses a low-spin, 6-coordinate Fe(II) heme with histidine and methionine as axial ligands.

MCD spectroscopy corroborates the assignment of the Fe(II)*Bx*RcoM-2 protein as a low-spin, 6-coordinate Fe(II) heme with two neutral axial ligands. The MCD spectrum of Fe(II) *Bx*RcoM-2, shown in Figure 4B, is dominated by an intense temperature-independent *A*-term in the α-β region with a crossover at 560 nm. Another, much less intense temperature-independent feature is observed in the Soret region with a crossover at 421 nm. The temperature independence of the MCD spectral features is consistent with an assignment of $S = 0$, low-spin, Fe(II) heme. The dominant *A*-term in the α-β region, also simply referred to as the alpha (α) band, is typical of Fe(II), low-spin heme systems, and its position is diagnostic for the type of axial ligation present (Table 3 and references therein). When cysteine(thiolate) is retained as a ligand after reduction, the α band crossover occurs between 562−576 nm, which can be observed for Fe(II)CBS at pH 9. When the sixth position is occupied by a neutral/non-thiolate ligand, the crossover position blue-shifts to ~550−560 nm, as observed in the Fe(II) states of *Rr*CooA and *Ec*Dos. The position of the α band in Fe(II)*Bx*RcoM-2 (560 nm), then, is in agreement with previous observations for other low-spin, 6-coordinate Fe(II) hemes (Table 3), which contain two neutral donor ligands.

The resonance Raman spectrum of Fe(II)*Bx*RcoM-2 (Figure 3B) shows oxidation, spin and coordination state vibrational modes consistent with the assignment of a low-spin, 6-coordinate heme. In the Fe(II) state, the heme axial ligands compete more effectively for the iron d_π orbitals, which is observed in lowered frequencies for the π-sensitive marker bands, of which ν_{11} is considered the most sensitive (33, 34). Fe(II)*Bx*RcoM-2 (Figure 3B) exhibits an oxidation state (ν_4) band at 1359 cm^{-1}, which is appropriately shifted to lower frequency from that of Fe(III)RcoM-2 (ν_4, 1371 cm^{-1}). The shoulder on ν_4 at 1368 cm^{-1} is attributed to a fraction of CO-bound protein that is present in the as-isolated protein (26). The spin and coordination state bands (ν_3 and ν_4) for Fe(II)*Bx*RcoM-2 occur at 1490 cm^{-1} and 1580 cm^{-1}. The 1490 cm^{-1} position of the spin state marker (ν_3) is indicative of a low spin system, and is at lower frequency than in Fe(III)*Bx*RcoM-2 (1500 cm^{-1}). The marker band ν_2, which overlaps with ν_{19}, is not shifted appreciably from its position in Fe(III)*Bx*RcoM-2; however, in Fe(II) *Bx*RcoM-2 ν_{10} is observed to shift to lower frequency (~1620 cm^{-1}), underneath a band associated with the $\nu_{C=C}$ porphyrin mode. The overlap of ν_{11} with ν_{38} decreases as ν_{11} shifts to lower frequency upon reduction of Fe(III)*Bx*RcoM-2, and this band is located at ~1536 cm^{-1} in the Fe(II)*Bx*RcoM-2 spectrum. The positions of all key marker bands in Fe(II) *Bx*RcoM-2 (Figure 3B) agree with expected values for low-spin, 6-coordinate Fe(II) heme proteins in which both ligands are neutral donors (33, 34). Importantly, these characteristic vibrational frequencies are not consistent with either a high spin state or the presence of cysteine (thiolate) as a heme iron ligand (43).

Characterization of the Fe(II)CO adduct of Bx*RcoM-2*

Electronic absorption and MCD spectra of Fe(II)CO *Bx*RcoM-2 (Figure 5) display features consistent with the formation of a 6-coordinate Fe(II)CO adduct with CO bound opposite a neutral ligand. In the presence of CO and reductant, the optical spectrum (Figure 5A) displays a slightly blue-shifted, very sharp and intense Soret feature at 423 nm. The sharp, inequivalent α-β peaks present in the Fe(II)*Bx*RcoM-2 spectrum are converted to a pair of nearly equivalent

peaks at ~540 and 570 nm. The order of CO addition and reduction does not appreciably influence the peak intensity ratio in the visible region. The same spectrum is obtained either when $CO_{(g)}$ is added to Fe(II)*Bx*RcoM-2 or when dithionite is added to Fe(III)*Bx*RcoM-2 in the presence of excess $CO_{(g)}$ (Figure 5A). The positions and shapes of the observed peaks in the UV and visible regions are typical for low-spin, 6-coordinate Fe(II)CO heme adducts (Supporting Information Table S2) in which CO binds opposite a neutral donor ligand. At 100 K, the MCD spectrum of Fe(II)CO *Bx*RcoM-2 (Figure 5B) is dominated by a derivative-shaped, temperature-independent *A*-term in the Soret region with a crossover at 423 nm and another temperature-independent feature in the α-β region with a crossover at 571 nm. At temperatures normally used in low temperature MCD (2−25 K), the CO adduct was susceptible to photolysis, which has been documented for other 6-coordinate CO-bound heme proteins (44). Comparison of the MCD peak positions (Supporting Information Table S2) with those of other 6-coordinate Fe(II)CO proteins shows a clear resemblance of Fe(II)CO *Bx*RcoM-2 to proteins with histidine as the axial ligand *trans* to CO.

Further characterization of Fe(II)CO *Bx*RcoM-2 utilized isotope-edited resonance Raman spectroscopy, as shown in Figure 6, to identify the Fe-CO and C-O stretching and bending modes to confirm the assignment of a 6-coordinate CO adduct with a *trans* histidine ligand. The binding of CO, a π acid ligand, to the Fe(II) heme is expected to compete with the porphryin macrocycle for iron d_π electrons, resulting in upshifts of π-sensitive marker bands toward Fe (III) frequencies as the porphyrin bonding modes strengthen. In Figure 6B, the marker bands that are sensitive to the Fe(II)CO oxidation, spin and coordination states, ν_4 (1368 cm^{-1}, ν_2 (1575 cm^{-1}), ν_3 (1494 cm^{-1} and ν_{10} (1630 cm^{-1}, are observed to shift relative to those of the Fe(II)*Bx*RcoM-2 spectrum. The frequencies of the major observed bands in Fe(II)CO *Bx*RcoM-2 (Figure 6B) are in agreement with other 6-coordinate CO-heme adducts with histidine as a *trans* ligand (45). Isotopic substitution with ^{13}CO identified the CO-associated stretching and bending modes, as shown in Figure 6A. The stretching modes (ν(Fe-^{12}CO), 485 cm^{-1}; ν(Fe-^{13}CO), 476 cm^{-1}) and bending modes (δ(Fe-^{12}CO), 565 cm^{-1}; δ(Fe-^{13}CO), 554 cm^{-1}) correlate well with those of known 6-coordinate Fe(II)CO proteins (Supporting Information Table S3 and references therein). In the high frequency region, modes for the coordinated C-O stretches (ν(^{12}C-O), 1965 cm^{-1}; ν(^{13}C-O), 1920 cm^{-1}) are also observed (Figure 6C). The Fe-CO and internal C-O stretching frequencies are linearly correlated with a negative coefficient; the ligand *trans* to CO also influences the observed frequencies of the two stretching modes (46,47). When the protein environment surrounding CO becomes more positive, π electrons are more highly delocalized from the Fe(II) to CO, strengthening the Fe-C bond, but weakening the C-O bond through increased population of the π* antibonding orbitals. The inverse is observed when the environment of the CO is more negative in nature. When the frequencies of the (Fe-CO) and (C-O) stretching modes are plotted on a ν(Fe-CO)/ν(C-O) correlation diagram (Supporting Information Figure S2), the values for *Bx*RcoM-2 are observed to fall near a cluster of values for other 6-coordinate Fe(II)CO heme proteins and related model complexes with histidine *trans* to CO. Furthermore, the position of Fe(II)CO *Bx*RcoM-2 on this correlation is consistent with a CO ligand which resides in a neutral, non-polar environment.

Characterization of the Fe(II)NO adduct of Bx*RcoM-2*

Electronic absorption spectroscopy of Fe(II)NO *Bx*RcoM-2 reveals spectral features (Figure 7) characteristic of a 6-coordinate Fe(II) NO-heme. As illustrated in Figure 7, upon addition of $NO_{(g)}$, the Soret absorption maximum of Fe(II)*Bx*RcoM-2 undergoes a blue shift from 425 nm to a slightly less intense, sharp Soret maximum at 422 nm, whose shape and position is comparable to that of known 6-coordinate Fe(II)NO heme proteins (Supporting Information Table S4). The transition of the α and β bands from the sharp, inequivalent peaks of the Fe(II) protein to the broader, more equivalent peaks at ~544 and 577 nm of the NO-adduct is observed

over several minutes (Figure 7) after a bolus of $NO_{(g)}$ is injected into the cuvette headspace. Five-coordinate NO-heme adducts, in which both endogenous ligands to iron have been displaced, display a broad, low intensity blue-shifted Soret typically at ~400 nm with α and β bands of approximately equivalent intensity (48). In contrast, 6-coordinate NO-hemes adducts, in which one endogenous ligand is retained opposite the NO, have distinct, sharp Soret bands with maxima in the 415−425 nm range (49). The shape and position of the observed Fe(II)NO Soret feature for *Bx*RcoM-2 in Figure 7 is clearly indicative of a 6-coordinate heme. Nitric oxide is also able to bind to Fe(III) hemes and induce reduction of heme to Fe(II) (50). In the case of *Bx*RcoM-2, the 6-coordinate Fe(II)NO adduct forms readily over 5−10 minutes after $NO_{(g)}$ is introduced into an anaerobic Fe(III)*Bx*RcoM-2 sample (data not shown). Anaerobic samples of Fe(II)CO *Bx*RcoM-2, however, remain relatively resistant to changes in coordination, even in the presence of a large excess of $NO_{(g)}$ (data not shown).

EPR spectroscopy of Fe(II)NO *Bx*RcoM-2 provides unambiguous confirmation of a 6-coordinate Fe(II) heme in which NO binds opposite a nitrogen-containing endogenous protein ligand. The observed rhombic spectrum for the ^{14}NO adduct of Fe(II)*Bx*RcoM-2, shown in Figure 8A, yields values of 1.976, 2.005 and 2.076 for g_x, g_y and g_z, respectively. The presence of a sixth nitrogen-containing ligand opposite the bound ^{14}NO gives rise to a rhombic splitting pattern in which nine lines are observed due to hyperfine and superhyperfine coupling between the unpaired electron on the nitrogen of the NO ligand and the proximal ligand nitrogen atom (51). In Fe(II)(^{14}NO) *Bx*RcoM-2, the observed hyperfine and superhyperfine coupling constants are measured at ~22.5 and ~7.5 Gauss, respectively. The observed *g* values and coupling constants for the Fe(II)(^{14}NO) adduct are similar to those of other 6-coordinate Fe(II)NO heme proteins (Supporting Information Table S5 and references therein). When isotopic substitution with ^{15}NO is performed (Figure 8B), hyperfine coupling of the unpaired electron with the I = ½ ^{15}N nucleus results in the expected shift to a six line spectrum with an increase in the hyperfine coupling constant to ~32.5 Gauss and a slight decrease in the superhyperfine coupling constant to ~6.5 Gauss; the *g* values remain consistent with those of the Fe(II)(^{14}NO) *Bx*RcoM-2. These signals are clearly distinct from those of 5-coordinate NO-heme adducts, which exhibit axially symmetric three-line spectra due to coupling of the electron with the single I = 1 ^{14}N nucleus of the bound NO; isotopically substituted 5-coordinate NO adducts have a hyperfine doublet due to the I = ½ ^{15}N nucleus (51). The observed EPR spectra (Figure 8, both isotopomers) of Fe(II)NO *Bx*RcoM-2 contain an additional feature at g_1~2.04 with a complementary feature presumed to occur near g_2~1.98, which was not resolved in these spectra. These features are found in other 6-coordinate Fe(II)NO adducts; the additional signals are attributed to alternate structures of His-Fe(II)-NO, which vary in Fe(II)-His and Fe(II)-NO distances and in the Fe(II)-N-O angle (52).

The assignment of a 6-coordinate Fe(II)NO *Bx*RcoM-2 adduct is also supported by resonance Raman data, which are shown in Supporting Information Figure S3. Modes sensitive to the Fe(II)NO oxidation, spin and coordination states, ν_4 (1371 cm^{-1}), ν_2 (1575 cm^{-1}), ν_3 (1496 cm^{-1}) and ν_{10} (1630 cm^{-1}) (Supporting Information Figure S3B), are in agreement with those of other 6-coordinate Fe(II)NO heme proteins; no additional features were observed for ν_3 to indicate the presence of 5-coordinate Fe(II)NO (53). In the low frequency region, isotopic substitution with ^{15}NO resolved a weak ν(Fe-NO) stretching mode (ν(Fe-^{14}NO), 565 cm^{-1}; ν(Fe-^{15}NO), 552 cm^{-1}) (Supporting Information Figure S3A). Isotopic substitution with ^{15}NO also results in the loss of a shoulder overlapping with ν_{10}, which we tentatively assign as the ν(^{14}N-O) band at 1631 cm^{-1} (Supporting Information Figure S3C). The ν(^{15}N-O) stretching mode, which would be expected at ~1600−1605 cm^{-1}, was obscured by porphyrin skeletal modes with excitation at 413.1, 406.7 and 530 nm, and cannot be assigned. The ν(Fe-^{14}NO) and tentative ν(^{14}N-O) frequencies correlate well with those of other 6-coordinate Fe(II)NO proteins with histidine *trans* to NO (Supporting Information Table S6). As with heme-CO adducts, the ν(Fe-NO) and ν(N-O) frequencies for proteins and model complexes are

correlated; Fe(II)NO adducts follow a less well-behaved 'anti-correlation' relationship (46). When the frequencies of ν(Fe-NO) and ν(N-O) for Fe(II)NO *Bx*RcoM-2 are plotted (Supporting Information Figure S4) with available protein and model complex data, Fe(II)NO *Bx*RcoM-2 falls near values for other 6-coordinate Fe(II)NO heme proteins and related model complexes with a neutral/histidine ligand *trans* to NO.

DISCUSSION

Functional studies of *Bx*RcoM-1 and *Bx*RcoM-2 implicate these proteins in aerobic CO-sensing (26). The *rcoM* genes reside adjacent to open reading frames encoding aerobic CO-oxidizing machinery, and in *in vivo* reporter assays, both *Bx*RcoM proteins drive CO-dependent transcription. Furthermore, in several organisms that lack a *cooA* gene, *rcoM* is found adjacent to the *coo* operon. These observations strongly suggest that RcoM serves as a CO sensing transcription factor analogous to CooA. However, the *Bx*RcoM proteins, with a heme-PAS domain and a LytR DNA-binding domain, are unrelated to CooA and utilize different heme coordination changes to transmit the CO signal. Our data suggest that the *B. xenovorans* RcoM proteins are also members of a more select group of heme-thiolate CO and NO gas-sensing proteins, which possess heme axial ligand environments that attenuate their sensing response to exclude regulation by O_2. As previously observed in *Rr*CooA (6), the *Bx*RcoM-2 heme appears tuned to sense CO as an effector ligand using a similar coordination environment and redox-dependent ligand switch (Scheme 1).

*Bx*RcoM-2 exhibits striking spectral similarities to other members of the heme-thiolate family of gas sensing proteins, including the heme-PAS sensor NPAS2. Resonance Raman and mutagenesis studies were used to identify the Fe(III) heme axial ligands of the NPAS2 PAS-A heme domain as Cys^{170} and His^{119} (54). Spectral comparison of *Bx*RcoM-2 to *Rr*CooA (37), NPAS-2 (54) and to other proteins with a neutral ligand opposite cysteine(thiolate) (55-57) suggest that a comparable coordination environment is present in *Bx*RcoM-2. For example, the narrow *g* anisotropy characteristic of heme-thiolate proteins that is observed for Fe(III)*Bx*RcoM-2 is similar to that seen for *Rr*CooA (37). The thiolate-coordinated hemes of *Bx*RcoM-2 and NPAS2 are distinct from those of the heme-containing PAS-domain proteins *Ec*Dos, FixL and *Ax*PDEA1. In both FixL and *Ax*PDEA1, the Fe(III) heme is high-spin and 5-coordinate, with a single conserved histidine ligand (3,14). *Ec*Dos, in contrast, is low-spin and 6-coordinate, with both the conserved histidine and a water (or hydroxide) coordinated to the heme iron (Scheme 1) (15).

Like *Rr*CooA and NPAS2, *Bx*RcoM-2 undergoes a ligand switch when reduced, replacing the cysteine(thiolate) axial ligand, as illustrated in Scheme 1. All the spectral characteristics of Fe(II)*Bx*RcoM-2 are indicative of a low-spin, 6-coordinate Fe(II) heme with two neutral donors, suggesting that the cysteine(thiolate) is no longer bound to the heme. Analogous replacement of a thiolate ligand upon reduction occurs in *Rr*CooA (22,23), where Cys^{75} is replaced by His^{77}, and in NPAS2, where Cys^{170} is replaced by His^{171} (54). In contrast, the O_2 sensing PAS-domain proteins FixL and *Ax*PDEA1 remain high-spin and 5-coordinate in the reduced state (3,14). Of the known gas sensing heme-PAS domain proteins, only *Ec*Dos is low-spin and 6-coordinate in both the Fe(III) and Fe(II) states; in the Fe(II) state, *Ec*Dos binds a methionine (Met^{95}) opposite histidine, which replaces a coordinated water (15). Fe(III)*Ec*Dos and Fe(III)*Bx*RcoM-2 differ considerably in their spectral characteristics (Tables 1 and 2); however, there are considerable similarities between these proteins in their reduced states. Comparison of Fe(II)*Ec*Dos and Fe(II)*Bx*RcoM-2 leads to the interesting observation that, while the position of the Soret band in Fe(II)*Bx*RcoM-2 is most similar those of proteins with two neutral nitrogen donors, i.e. *Rr*CooA (58) and neuroglobin (59), the positions of the α and β peaks are most similar to those of *Ec*Dos (4) (Table 3).

The identity of potential ligands in the *Bx*RcoM proteins was inferred by sequence comparison among a related set of heme-PAS proteins and verified by mutational analysis (26). Alignment of the PAS domains of *Bx*RcoM-2, its homolog *Bx*RcoM-1, FixL proteins from two organisms, and *Ec*Dos suggested that His^{74} in the *Bx*RcoM proteins was a heme ligand candidate. Mutational analysis corroborated this proposal: in *Bx*RcoM-1 alteration of His^{74} eliminated accumulation of heme-bound protein. The spectral data on *Bx*RcoM-2 presented herein strongly suggest that histidine, presumably His^{74}, is a ligand in both the Fe(III) and Fe(II) states. Our data further reveal that *Bx*RcoM-2 undergoes a redox-mediated ligand switch in which the cysteine(thiolate) ligand is replaced by a neutral donor. In the *Bx*RcoM proteins there are only three cysteines, Cys^{94}, Cys^{127}, Cys^{130}; studies are underway to identify which of these is the axial ligand to the Fe(III) heme. By analogy to *Rr*CooA and NPAS2, we would expect a nearby neutral residue to replace cysteine in the Fe(II) state. A model for Fe(II)*Bx*RcoM-1, using the structure of Fe(II)*Ec*Dos (17) as a template, placed either Met^{104} or Met^{105} in close proximity to the heme. Variants at Met^{104}, but not Met^{105}, altered *Bx*RcoM-1 visible spectral and functional behavior (26), consistent with the conclusion that Met^{104} serves as a ligand to the Fe(II) heme. The observed spectroscopic data are consistent with, though not conclusive evidence for, the presence of the analogous Met^{104} ligand in Fe(II)*Bx*RcoM-2.

When Fe(II)*Bx*RcoM-2 binds CO, we infer that His^{74} is retained as the sixth ligand, while Met^{104} is replaced by CO (Scheme 1). The spectral features of Fe(II)CO *Bx*RcoM-2 in the electronic absorption, MCD and resonance Raman spectra (Supporting Information Table S2 and S3) are all consistent with the presence of histidine *trans* to CO. The observed Fe-CO and C-O stretching frequencies, when plotted on a correlation diagram (46), place *Bx*RcoM-2 on the correlation line for histidine as the *trans* ligand, near a cluster of His/CO heme adducts that includes *Ec*Dos (Supporting Information Figure S3). Furthermore, the correlation position indicates that the CO ligand is bound in a neutral/non-polar environment in *Bx*RcoM-2 (45, 47), suggesting that the *Bx*RcoM-2 heme-PAS domain is comparable in hydrophobicity to those of FixL and *Ec*Dos (17,60). In contrast, *Rr*CooA has a C-O stretching frequency that is upshifted considerably (Supporting Information Figure S3) (61).

Despite the strong negative *trans* influence of NO (62), which thermodynamically favors a 5-coordinate NO-heme adduct, Fe(II)*Bx*RcoM-2 forms a 6-coordinate nitrosyl adduct. EPR of the isotopically labelled ^{14}NO and ^{15}NO adducts reveal the presence of superhyperfine coupling that can only arise from the coordination of a nitrogen atom opposite the NO ligand at the heme iron. The most likely source of this nitrogen is His^{74}, suggesting that Met^{104} is the ligand that is replaced upon gas binding. The presence of a 6-coordinate nitrosyl in the heme-PAS domain sensor proteins has precedent; the FixLs have been shown to form a temperature dependent mixture of 5- and 6-coordinate NO-adducts, and the 6-coordinate NO adduct is favored by both *Ax*PDEA1 and *Ec*Dos (63). Interestingly, in all heme-thiolate proteins thus far characterized, including *Rr*CooA (58), hCBS (64) and NPAS2 (PAS-A) (54), NO coordination to the heme iron causes the displacement of both axial ligands to form a 5-coordinate NO adduct. Furthermore, the formation of the 5-coordinate NO adduct in *Rr*CooA results in inactivation of the protein, which implies that retention of the proximal histidine ligand is required for transcriptional activation in *Rr*CooA (58). It is not yet clear what effect or relevance, if any, the binding of NO to form a 6-coordinate adduct has on the DNA-binding activity of *Bx*RcoM-1 or *Bx*RcoM-2.

Patterns are now evident that illuminate how heme-based sensors discriminate among the three diatomic gases that serve as signals in a variety of cellular systems: O_2, NO and CO. In the O_2 sensing PAS-domain proteins, as in hemoglobin and myoglobin, the Fe(II) heme is 5-coordinate and high spin, with a single histidine ligand (13,65). The binding of O_2 to form a 6-coordinate complex induces a spin state change, which alters local steric interactions and drives a global conformational change. In the FixL proteins, specificity for O_2 arises from

interactions of the bound O_2 ligand with a conserved arginine residue via hydrogen bonding. Hydrogen bond donation to bound O_2, as originally observed in the globins, appears to be a common selection mechanism for O_2. In the H-NOX proteins, which are either O_2 or NO sensors, a distal pocket tyrosine is required to select for O_2 binding (66,67). The tyrosine traps the bound O_2, which would otherwise dissociate too rapidly to form a complex; H-NOX proteins without this tyrosine exhibit low affinities for O_2 and are NO sensors. Trans ligand influences amplify this discrimination: the O_2 sensing proteins form a 6-coordinate NO adduct, which is thermodynamically less favorable, while NO sensors form the thermodynamically preferred 5-coordinate NO adduct. The H-NOX family member soluble guanylyl cyclase employs this strategy to bind NO with a high degree of discrimination against O_2 (68), and displacement of the *trans* histidine ligand to form the 5-coordinate NO adduct induces enzyme activation (69). CO, which activates soluble guanylyl cyclase only weakly, forms 6-coordinate adduct with retention of the histidine (68).

*Rr*CooA uses this 5- and 6-coordination number difference to selectively respond to CO. *Rr*CooA is only active when CO forms a 6-coordinate adduct; the 5-coordinate NO adduct is inactive for DNA binding (58). A CooA homolog from the thermophilic bacterium *C. hydrogenoformans* (*Ch*CooA) forms 6-coordinate NO and CO adducts at room temperature, both of which are active for DNA binding (70). At temperatures relevant to the physiological environment of the bacterium, the 6-coordinate NO adduct reversibly converts to a 5-coordinate NO adduct, suggesting that CO is the physiologically relevant regulator. Further selectivity for CO arises from the unique coordination properties of *Rr*CooA that preclude formation of an O_2 adduct. The Fe(II) protein is 6-coordinate, and only the strongly binding ligands NO and CO are able to replace the endogenous proline ligand. Furthermore, ligand switching between the Fe(II) and Fe(III) states ensures that the heme is oxidized by O_2, as the Fe(III) heme is stabilized by its cysteine(thiolate) ligand.

Our data support a mechanism in which the *Bx*RcoM proteins utilize selective ligand replacement to respond to CO, as illustrated in Scheme 1. The heme environment of *Bx*RcoM-2 shares similarities with both *Rr*CooA and the heme-PAS gas sensor *Ec*Dos. Similar to *Rr*CooA, the Fe(III) heme of *Bx*RcoM-2 is 6-coordinate and low spin with a cysteine(thiolate) as one of the ligands, and this cysteine(thiolate) is lost upon reduction. Like *Ec*Dos (16,17), the new ligand in the Fe(II) state of *Bx*RcoM-2 is likely to be methionine. *Ec*Dos is unique among the heme-PAS gas sensors in requiring the rupture of a heme iron-ligand bond in order to bind a gas molecule, and Met^{95} is the ligand that is replaced when gases bind. In the FixLs, *Ax*PDEA1 and *Ec*Dos , a conserved arginine provides important hydrogen-bonding contacts when O_2 binds (12); this residue is not conserved in the *Bx*RcoM proteins (26). The absence of this key O_2 interaction in the *Bx*RcoMs is consistent with a role in CO-sensing. In *Bx*RcoM-2, as in *Ec*Dos, the methionine ligand is more weakly bound than the histidine ligand, and therefore it is the methionine that is selectively replaced upon effector binding. This ligand replacement is similar to that of *Rr*CooA, in which the more weakly bound proline ligand is selectively replaced upon binding CO (21,71).

CONCLUSION

Previous work by Kerby, *et al*. (26) and the work described herein demonstrate that *Bx*RcoM-2 and, by analogy, *Bx*RcoM-1, possess features similar to those of the well-characterized heme-thiolate CO-sensor CooA and the heme-PAS domain gas-sensing protein *Ec*Dos, which require the replacement of an endogenous ligand for gas binding. Based on the results of these studies, we propose that the resting state of Fe(III)*Bx*RcoM-2 is low-spin and 6-coordinate with His^{74}/Cys^{xx} axially coordinated. Reduction results in the replacement of Cys^{xx} with a nearby methionine (Met^{104}), which is then itself replaced when CO binds opposite His^{74}. Although replacement of His^{74} by CO is plausible, Met_{104} retention is not consistent with our observation

that NO binds opposite an endogenous nitrogen-donor ligand. By analogy to other 6-coordinate heme-based sensors, *Ec*Dos and *Rr*CooA, we propose that methionine serves in the *Bx*RcoM proteins as a less avidly bound ligand, which is preferentially replaced by the CO effector molecule.

Supplementary Material

Refer to Web version on PubMed Central for supplementary material.

Acknowledgments

The authors would like to express thanks to Professor Thomas C. Brunold and his research group for their expertise and the generous use of their instrumentation. The authors also thank Dr. Frank Neese (MPI Mülheim) for the WEPR spectral fitting program.

ABBREVIATIONS

*Ax*PDEA1	*Acetobacter xylinum* phosphodiesterase A1
BMAL1	brain and muscle Arnt-like protein 1
CCP	cytochrome *c* peroxidase
*Ch*CooA	a CooA homologue from the thermophilic bacterium *Carboxydothermus hydrogenoformans*
CO	carbon monoxide
*Rr*CooA	a heme-containing CO-sensing transcriptional factor in *Rhodospirillum rubrum*
CPO	chloroperoxidase
*Ec*Dos	direct oxygen sensor in *Escherichia coli*
EPPS	3-[4-(2-hydroxyethyl)-1-piperazinyl]propanesulfonic acid
FixL	an O_2-sensing heme protein that regulates expression of genes associated with N_2 fixation
EPR	electronic paramagnetic resonance
hCBS	human cystathionine β-synthase, a heme-containing pyridoxal 5'-phosphate enzyme
HemAT	heme-based aerotactic transducer in *Bacillus subtilis*, an oxygen sensor
HRP	horseradish peroxidase
M80C cyt *c*	cytochrome *c* variant in which methionine is replaced by cysteine(thiolate) as an axial ligand to the Fe(III) heme
MCD	magnetic circular dichroism
MOPS	3-(N-morpholino)propanesulfonic acid
NO	nitric oxide
NPAS2	neuronal PAS domain protein 2, a heme-containing CO-responsive eukaryotic transcriptional regulator
$P450_{CAM}$	camphorhydroxylating cytochrome P450 from *Pseudomonas putida*
$P450_{CAM}$+ImH	$P450_{CAM}$ with imidazole as an axial ligand to the Fe(III) heme

PAS	a domain structure named for the proteins in which the motif was first identified, Period, aryl hydrocarbon receptor nuclear translocator (ARNT), Simple-minded proteins
RCCP	*Rhodobacter capsulatus* cytochrome *c*’
sGC	soluble guanylyl cyclase, an NO-sensing heme protein that catalyzes the conversion of GTP to cGMP

REFERENCES

1. Gilles-Gonzalez M-A, Gonzalez G. Heme-based sensors: Defining characteristics, recent developments, and regulatory hypotheses. J. Inorg. Biochem 2005;99:1–22. [PubMed: 15598487]
2. Jain R, Chan MK. Mechanisms of ligand discrimination by heme proteins. J. Biol. Inorg. Chem 2003;8:1–11. [PubMed: 12459893]
3. Gilles-Gonzalez MA, Gonzalez G, Perutz MF, Kiger L, Marden MC, Poyart C. Heme-based sensors, exemplified by the kinase FixL, are a new class of heme protein with distinctive ligand binding and autooxidation. Biochemistry 1994;33:8067–8073. [PubMed: 8025112]
4. Delgado-Nixon VM, Gonzalez G, Gilles-Gonzalez M-A. Dos, a heme-binding PAS protein from *Escherichia coli*, is a direct oxygen sensor. Biochemistry 2000;39:2685–2691. [PubMed: 10704219]
5. Hou S, Larsen RW, Boudko D, Riley CW, Karatan E, Zimmer M, Ordal GW, Alam M. Myoglobin-like aerotaxis transducers in archaea and bacteria. Nature 2000;403:540–544. [PubMed: 10676961]
6. Roberts GP, Kerby RL, Youn H, Conrad M. CooA, a paradigm for gas sensing regulatory proteins. J. Inorg. Biochem 2005;99:280–292. [PubMed: 15598507]
7. Dioum EM, Rutter J, Tuckerman JR, Gonzalez G, Gilles-Gonzalez M-A, Mcknight SL. NPAS2: a gas-responsive transcription factor. Science 2002;298:2385–2387. [PubMed: 12446832]
8. Arnold WP, Mittal CK, Katsuki S, Murad F. Nitric oxide activates guanylate cyclase and increases guanosine 3′, 5′-cyclic monophosphate levels in various tissue preparations. Proc. Natl. Acad. Sci. USA 1977;74:3203–3207. [PubMed: 20623]
9. Karow DS, Pan D, Tran R, Pellicena P, Presley A, Mathies RA, Marletta MA. Spectroscopic characterization of the soluble guanylate cyclase-like heme domains from *Vibrio cholerae* and *Thermoanaerobacter tengcongensis*. Biochemistry 2004;43:10203–10211. [PubMed: 15287748]
10. Gu YZ, Hogenesch JB, Bradfield CA. The PAS superfamily: sensors of environmental and developmental signals. Annu. Rev. Pharmacol. Toxicol 2000;40:519–561. [PubMed: 10836146]
11. David M, Daveran ML, Batut J, Dedieu A, Domergue O, Ghai J, Hertig C, Boistard P, Kahn D. Cascade regulation of *nif* gene expression in *Rhizobium meliloti*. Cell 1988;54:671–683. [PubMed: 2842062]
12. Dunham CM, Dioum EM, Tuckerman JR, Gonzalez G, Scott WG, Gilles-Gonzalez MA. A distal arginine in oxygen-sensing heme-PAS domains is essential to ligand binding, signal transduction, and structure. Biochemistry 2003;42:7701–7708. [PubMed: 12820879]
13. Tuckerman JR, Gonzalez G, Dioum EM, Gilles-Gonzalez MA. Ligand and oxidation-state specific regulation of the heme-based oxygen sensor FixL from *Sinorhizobium meliloti*. Biochemistry 2002;41:6170–6177. [PubMed: 11994013]
14. Chang AL, Tuckerman JR, Gonzalez G, Mayer R, Weinhouse H, Volman G, Amikam D, Benziman M, Gilles-Gonzalez MA. Phosphodiesterase A1, a regulator of cellulose synthesis in *Acetobacter xylinum*, is a heme-based sensor. Biochemistry 2001;40:3420–3426. [PubMed: 11297407]
15. Sasakura Y, Yoshimura-Suzuki T, Kurokawa H, Shimizu T. Structure-function relationships of *Ec*DOS, a heme-regulated phosphodiesterase from *Escherichia coli*. Acc. Chem. Res 2006;39:37–43. [PubMed: 16411738]
16. Tanaka A, Takahashi H, Shimizu T. Critical role of the heme axial ligand, Met95, in locking catalysis of the phosphodiesterase from *Escherichia coli* (*Ec*DOS) toward cyclic diGMP. J. Biol. Chem 2007;282:21301–21307. [PubMed: 17535805]

17. Kurokawa H, Lee DS, Watanabe M, Sagami I, Mikami B, Raman CS, Shimizu T. A redox-controlled molecular switch revealed by the crystal structure of a bacterial heme PAS sensor. J. Biol. Chem 2004;279:20186–20193. [PubMed: 14982921]
18. Reick M, Garcia JA, Dudley C, Mcknight SL. NPAS2: an analog of clock operative in the mammalian forebrain. Science 2001;293:506–509. [PubMed: 11441147]
19. Aono S. Biochemical and biophysical properties of the CO-sensing transcriptional activator CooA. Acc. Chem. Res 2003;36:825–831. [PubMed: 14622029]
20. Lanzilotta WN, Schuller DJ, Thorsteinsson MV, Kerby RL, Roberts GP, Poulos TL. Structure of the CO-sensing transcription activator CooA. Nat. Struct. Biol 2000;7:876–880. [PubMed: 11017196]
21. Clark RW, Youn H, Parks RB, Cherney MM, Roberts GP, Burstyn JN. Investigation of the role of the N-terminal proline, the distal ligand in the CO sensor CooA. Biochemistry 2004;43:14149–14160. [PubMed: 15518565]
22. Shelver D, Thorsteinsson MV, Kerby RL, Chung S-Y, Roberts GP, Reynolds MF, Parks RB, Burstyn JN. Identification of two important heme site residues (Cysteine 75 and Histidine 77) in CooA, the CO-sensing transcription factor of *Rhodospirillum rubrum*. Biochemistry 1999;38:2669–2678. [PubMed: 10052937]
23. Aono S, Ohkubo K, Matsuo T, Nakajima H. Redox-controlled ligand exchange of the heme in the CO-sensing transcriptional activator CooA. J. Biol. Chem 1998;273:25757–25764. [PubMed: 9748246]
24. Kerby RL, Youn H, Thorsteinsson MV, Roberts GP. Repositioning about the dimer interface of the transcription regulator CooA: A major signal transduction pathway between the effector and DNA-binding domains. J. Mol. Biol 2003;325:809–823. [PubMed: 12507482]
25. Coyle CM, Puranik M, Youn H, Nielsen SB, Williams RD, Kerby RL, Roberts GP, Spiro TG. Activation mechanism of the CO sensor CooA: Mutational and resonance Raman spectroscopic studies. J. Biol. Chem 2003;278:35384–35393. [PubMed: 12796503]
26. Kerby RL, Youn H, Roberts GP. RcoM: A new single-component transcriptional regulator of CO metabolism in bacteria. J. Bacteriol 2008;190:3336–3343. [PubMed: 18326575]
27. Chain PSG, Denef VJ, Konstantinidis KT, Vergez LM, Agullo L, Reyes VL, Hauser L, Cordova M, Gomez L, Gonzalez M, Land M, Lao V, Larimer F, Lipuma JJ, Mahenthiralingam E, Malfatti SA, Marx CJ, Parnell JJ, Ramette A, Richardson P, Seegerg M, Smith D, Spilker T, Sul WJ, Tsoi TV, Ulrich LE, Zhulin IB, Tiedje JM. *Burkholderia xenovorans* LB400 harbors a multi-replicon, 9.73-Mbp genome shaped for versatility. Proc. Natl. Acad. Sci. USA 2006;103:15280–15287. [PubMed: 17030797]
28. Dykxhoorn DM, Pierre RS, Linn T. Synthesis of the end subunits of *Escherichia coli* RNA polymerase is autogenously regulated *in vivo* by both transcriptional and translational mechanisms. Gene 1996;177:133–136. [PubMed: 8921858]
29. Waterman MR. Spectral characterization of human hemoglobin and its derivatives. Meth. Enzymol 1978;52:456–463. [PubMed: 672648]
30. Neese, F. Electronic structure and spectroscopy of novel copper chromophores in biology. University of Konztanz; Germany: 1997.
31. Abe M, Kitagawa T, Kyogoku Y. Resonance Raman spectra of octaethylporphyrinato-Ni(II) and *meso*-deuterated and ^{15}N substituted derivatives. II. A normal coordinate analysis. J. Chem. Phys 1978;69:4526–4534.
32. Woodruff WH, Adams DH, Spiro TG, Yonetani T. Resonance Raman spectra of cobalt myoglobins and cobalt porphyrins. Evaluation of protein effects on porphyrin structure. J. Am. Chem. Soc 1975;97:1695–1698. [PubMed: 1133400]
33. Spiro TG. Resonance Raman spectroscopic studies of heme proteins. Biochim. Biophys. Acta 1975;416:169–189. [PubMed: 169917]
34. Spiro TG, Strekas TC. Resonance Raman spectra of heme proteins. Effects of oxidation and spin state. J. Am. Chem. Soc 1974;96:338–345. [PubMed: 4361043]
35. Dawson JH, Andersson LA, Sono M. Spectroscopic investigations of ferric cytochrome P-450_{CAM} ligand complexes. J. Biol. Chem 1982;257:3606–3617. [PubMed: 6277939]
36. Pazicni, S. Department of Chemistry. University of Wisconsin-Madison; Madison, Wisconsin: 2006. Towards understanding the role of the heme cofactor in cystathionine β-synthase; p. 292

37. Reynolds MF, Shelver D, Kerby RL, Parks RB, Roberts GP, Burstyn JN. EPR and electronic absorption spectroscopies of the CO-sensing CooA protein reveal a cysteine-ligated low-spin ferric heme. J. Am. Chem. Soc 1998;120:9080–9081.
38. Omura T, Sadano Hiroyuki, Hasegawa Tohru, Yoshida Yuzo, Kominami Shiro. Hemoprotein H-450 identified as a form of cytochrome P-450 having an endogenous ligand at the 6th coordination position of the heme. J. Biochem 1996;96:1491–1500. [PubMed: 6098577]
39. Blumberg WE, Peisach J. Low-spin compounds of heme proteins. Adv. Chem. Ser 1971;100:271–291.
40. Desbois A, Lutz M, Banerjee R. Low-frequency vibrations in resonance Raman spectra of horse heart myoglobin. Iron-ligand and iron-nitrogen vibration models. Biochemistry 1979;18:1510–1518. [PubMed: 427129]
41. Champion PM, Stallard BR, Wagner GC, Gunsalus IC. Resonance Raman detection of an Fe-S bond in cytochrome $P450_{CAM}$. J. Am. Chem. Soc 1982;104:5469–5472.
42. Green EL, Taoka S, Banerjee R, Loehr TM. Resonance Raman characterization of the heme cofactor in cystathionine β-synthase. Identification of the Fe-S(Cys) vibration in the six-coordinate low-spin heme. Biochemistry 2001;40:459–463. [PubMed: 11148040]
43. Champion PM, Gunsalus IC, Wagner GC. Resonance Raman investigations of cytochrome $P450_{CAM}$ from *Pseudomonas putida*. J. Am. Chem. Soc 1978;100:3743–3751.
44. Brittain T, Greenwood C, Springall J, Thomson AJ. The nature of ferrous haem protein complexes prepared by photolysis. Biochim. Biophys. Acta 1982;703:117–128.
45. Tsubaki M, Srivastava RB, Yu N-T. Resonance Raman investigation of carbon monoxide bonding in (carbonmonoxy)hemoglobin and -myoglobin: Detection of Fe-CO stretching and Fe-C-O bending vibrations and influence of quaternary structure change. Biochemistry 1982;21:1132–1140. [PubMed: 7074069]
46. Ibrahim M, Xu C, Spiro TG. Differential sensing of protein influences by NO and CO vibrations in heme adducts. J. Am. Chem. Soc 2006;128:16834–16845. [PubMed: 17177434]
47. Vogel KM, Kozlowski PM, Zgierski MZ, Spiro TG. Determinants of the FeXO [X=C,N,O] vibrational frequencies in heme adducts from experiment and density functional theory. J. Am. Chem. Soc 1999;121:9915–9921.
48. Stone JR, Sands RH, Dunham WR, Marletta MA. Electron paramagnetic resonance evidence for the formation of a pentacoordinate nitrosyl-heme complex in soluble guanylate cyclase. Biochem. Biophys. Res. Commun 1995;207:572–577. [PubMed: 7864845]
49. Yoshimura T, Ozaki T. Electronic spectra for nitrosyl(protoporphyrin IX dimethyl ester)iron(II) and its complexes with nitrogenous bases as model systems for nitrosylhemoproteins. Arch. Biochem. Biophys 1984;229:126–135. [PubMed: 6703691]
50. Addison AW, Stephanos JJ. Nitrosyliron(III) hemoglobin: Autoreduction and spectroscopy. Biochemistry 1986;25:4104–4113. [PubMed: 3741844]
51. Palmer, G. Electron paramagnetic resonance of hemoproteins. In: Lever, ABP.; Gray, HB., editors. Iron Porphyrins. Addison-Wesley; Reading, Massachusetts: 1983. p. 43-88.
52. Morse RH, Chan SI. Electron paramagnetic resonance studies of nitrosyl ferrous heme complexes: Determination of an equilibrium between two conformations. J. Biol. Chem 1980;255:7876–7882. [PubMed: 6249819]
53. Mackin HC, Benko B, Yu NT, Gersonde K. Resonance Raman study on pentacoordinated and hexacoordinated ferrous nitrosyl myoglobin. The influence of pH. FEBS Lett 1983;158:199–202.
54. Uchida T, Sato E, Sato A, Sagami I, Shimizu T, Kitagawa T. CO-dependent activity-controlling mechanism of heme-containing CO-sensor protein, neuronal PAS domain protein 2. J. Biol. Chem 2005;280:21358–21368. [PubMed: 15797872]
55. Lipscomb JD. Electron paramagnetic resonance detectable states of cytochrome $P\text{-}450_{CAM}$. Biochemistry 1980;19:3590–3599. [PubMed: 6250573]
56. Pazicni S, Lukat-Rodgers GS, Oliveriusova J, Rees KA, Parks RB, Clark RW, Rodgers KR, Kraus JP, Burstyn JN. The redox behavior of the heme is cystathionine β-synthase is sensitive to pH. Biochemistry 2004;43:14684–14695. [PubMed: 15544339]
57. Wuttke, DS. Preparation, characterization and intramolecular electron transfer studies of ruthenium-modified cytochromes *c*. California Institute of Technology; Pasadena, California: 1993. p. 408-413.

58. Reynolds MF, Parks RB, Burstyn JN, Shelver D, Thorsteinsson MV, Kerby RL, Roberts GP, Vogel KM, Spiro TG. Electronic absorption, EPR and resonance Raman spectroscopies of CooA, a CO-sensing transcription factor from *R. rubrum*, reveals a five-coordinate NO-heme. Biochemistry 2000;39:388–396. [PubMed: 10631000]
59. Dewilde S, Kiger L, Burmester T, Hankeln T, Baudin-Creuza V, Aerts T, Marden MC, Caubergs R, Moens L. Biochemical characterization and ligand binding properties of neuroglobin, a novel member of the globin family. J. Biol. Chem 2001;276:38949–38955. [PubMed: 11473128]
60. Key J, Moffat K. Crystal structure of deoxy and CO-bound *Bj*FixLH reveal details of ligand recognition and signaling. Biochemistry 2005;44:4627–4635. [PubMed: 15779889]
61. Uchida T, Ishikawa H, Takahashi S, Ishimori K, Morishima I, Ohkubo K, Nakajima H, Aono S. Heme environmental structure of CooA is modulated by the target DNA binding. Evidence from resonance Raman spectroscopy and CO rebinding kinetics. J. Biol. Chem 1998;273:19988–19992. [PubMed: 9685335]
62. Traylor TG, Sharma VS. Why NO? Biochemistry 1992;31:2847–2849. [PubMed: 1348002]
63. Tomita T, Gonzalez G, Chang AL, Ikeda-Saito M, Gilles-Gonzalez MA. A comparative resonance Raman analysis of heme-binding PAS domains: Heme iron coordination structures of the *Bj*FixL, *Ax*PDEA1, *Ec*Dos, and *Mt*Dos proteins. Biochemistry 2002;41:4819–4826. [PubMed: 11939776]
64. Taoka S, Banerjee R. Characterization of NO binding to human cystathionine β-synthase: Possible implications of the effects of CO and NO binding to the human enzyme. J. Inorg. Biochem 2001;87:245–251. [PubMed: 11744062]
65. Hao B, Isaza C, Arndt J, Soltis M, Chan MK. Structure-based mechanism of O_2 sensing and ligand discrimination by the FixL heme domain of *Bradyrhizobium japonicum*. Biochemistry 2002;41:12952–12958. [PubMed: 12390021]
66. Nioche P, Berka V, Vipond J, Minton N, Tsai A-L, Raman CS. Femtomolar sensitivity of a NO sensor from *Clostridium botulinum*. Science 2004;306:1550–1553. [PubMed: 15472039]
67. Boon EM, Marletta MA. Ligand discrimination in soluble guanylate cyclase and the H-NOX family of heme sensor proteins. Curr. Opin. Chem. Biol 2005;9:441–446. [PubMed: 16125437]
68. Burstyn JN, Yu AE, Dierks EA, Hawkins BK, Dawson JH. Studies of the heme coordination and ligand binding properties of soluble guanylyl cyclase(sGC): Characterization of Fe(II)sGC and Fe (II)sGC(CO) by electronic absorption and magnetic circular dichroism spectroscopies and failure of CO to activate the enzyme. Biochemistry 1995;34:5896–5903. [PubMed: 7727447]
69. Dierks EA, Burstyn JN. Nitric oxide (NO.), the only nitrogen monoxide redox form capable of activating soluble guanylyl cyclase. Biochem. Pharmacol 1996;51:1593–1600. [PubMed: 8687474]
70. Clark RW, Lanz ND, Lee AJ, Kerby RL, Roberts GP, Burstyn JN. Unexpected NO-dependent DNA binding by the CooA homolog from *Carboxydothermus hydrogenoformans*. Proc. Natl. Acad. Sci. USA 2006;103:891–896. [PubMed: 16410360]
71. Pinkert J, Clark RW, Burstyn JN. Modeling proline ligation in the heme-dependent CO sensor, CooA, using molecule analogs. J. Biol. Inorg. Chem 2006;5:642–650. [PubMed: 16724227]
72. Lu Y, Casimiro DR, Bren KL, Richards JH, Gray HB. Structurally engineered cytochromes with unusual ligand-binding properties: expression of *Saccharomyces cerevisiae* Met-80-Ala iso-1-cytochrome *c*. Proc. Natl. Acad. Sci. USA 1993;90:11456–11459. [PubMed: 8265573]
73. Banci, L.; Assfalg, M. Mitochondrial cytochrome *c*. In: Messerschmidt, AH,R.; Poulos, T.; Weighardt, K., editors. Handbook of Metalloproteins. John Wiley and Sons; Chichester: 2001. p. 33-43.
74. Hirata S, Matsui T, Sasakura Y, Sugiyama S, Yoshimura T, Sagami I, Shimizu T. Characterization of Met95 mutants of a heme-regulated phosphodiesterase from *Escherichia coli*. Optical absorption, magnetic circular dichroism, circular dichroism, and redox potentials. Eur. J. Biochem 2003;270:4771–4779. [PubMed: 14622266]
75. Mathews, FS. *b*-Type cytochrome electron carriers: cytochromes b_{562} and b_5, and flavocytochrome b_2. In: Messerschmidt, AH,R.; Poulos, T.; Weighardt, K., editors. Handbook of Metalloproteins. John Wiley and Sons; Chichester: 2001. p. 33-43.
76. Gonzalez G, Dioum EM, Bertolucci CM, Tomita T, Ikeda-Saito M, Cheesman MR, Watmough NJ, Gillez-Gonzalez M-A. Nature of the displaceable heme-axial residue in the *Ec*Dos protein, a heme-based sensor from *Escherichia coli*. Biochemistry 2002;41:8414–8421. [PubMed: 12081490]

77. Boiss-Poltoratzsky R, Ehrenberg A. Magnetic and spectrophotometric investigations of cytochrome b_5. Eur. J. Biochem 1967;2:361–365. [PubMed: 4294947]

78. Nistor SV, Goovaerts E, Van Doorslaer S, Dewilde S, Moens L. EPR-spectroscopic evidence of a dominant His–Fe III–His coordination in ferric neuroglobin. Chem. Phys. Lett 2002;361:355–361.

79. Margoliash E, Frohwirt N. Spectrum of horse-heart cytochrome *c*. B*iochem. J.* 1959;71:570–572. [PubMed: 13638266]

80. Vickery L, Salmon A, Sauer K. Magnetic circular dichroism studies on microsomal aryl hydrocarbon hydroxylase: Comparison with cytochrome b_5 and cytochrome P-450_{CAM}. Biochim. Biophys. Acta 1975;386:87–98. [PubMed: 164936]

81. Dhawan IK, Shelver D, Thorsteinsson MV, Roberts GP, Johnson MK. Probing the heme axial ligation in the CO-sensing CooA protein with magnetic circular dichroism spectroscopy. Biochemistry 1999;38:12805–12813. [PubMed: 10504250]

82. Vickery L, Nozawa T, Sauer K. Magnetic circular dichroism studies of low-spin cytochromes. Temperature dependence and effects of axial coordination of the spectra of cytochrome *c* and cytochrome b_5. J. Am. Chem. Soc 1976;98:351–357. [PubMed: 1438]

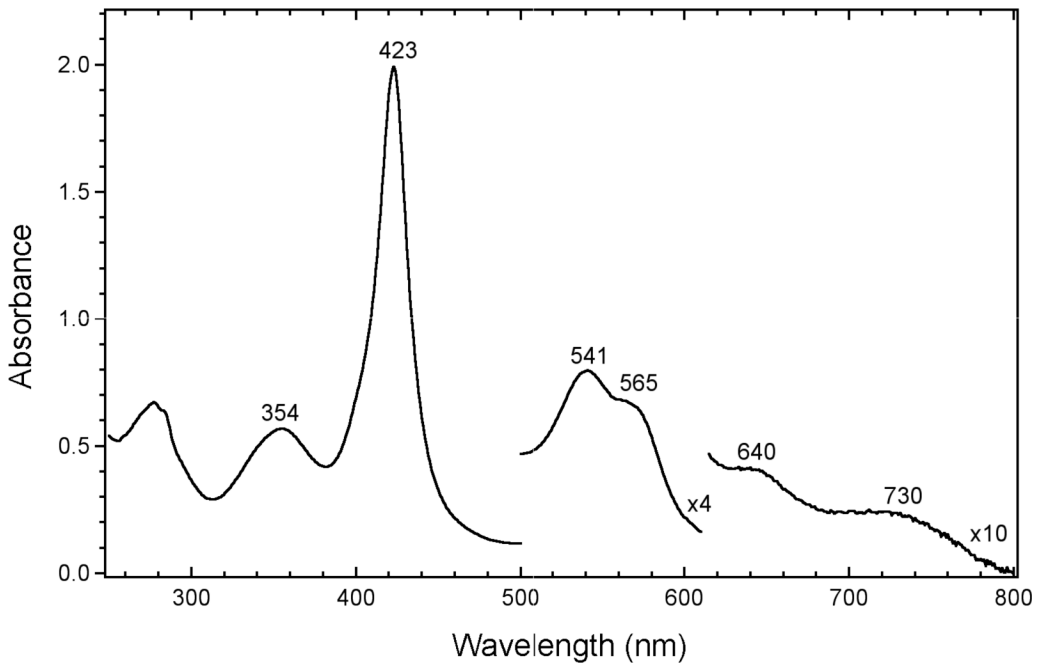

Figure 1.
Electronic absorption spectrum of purified Fe(III)*Bx*RcoM-2. The sample was 12 μM heme in 25 mM EPPS buffer with 500 mM KCl, pH 8.0, at 25 °C.

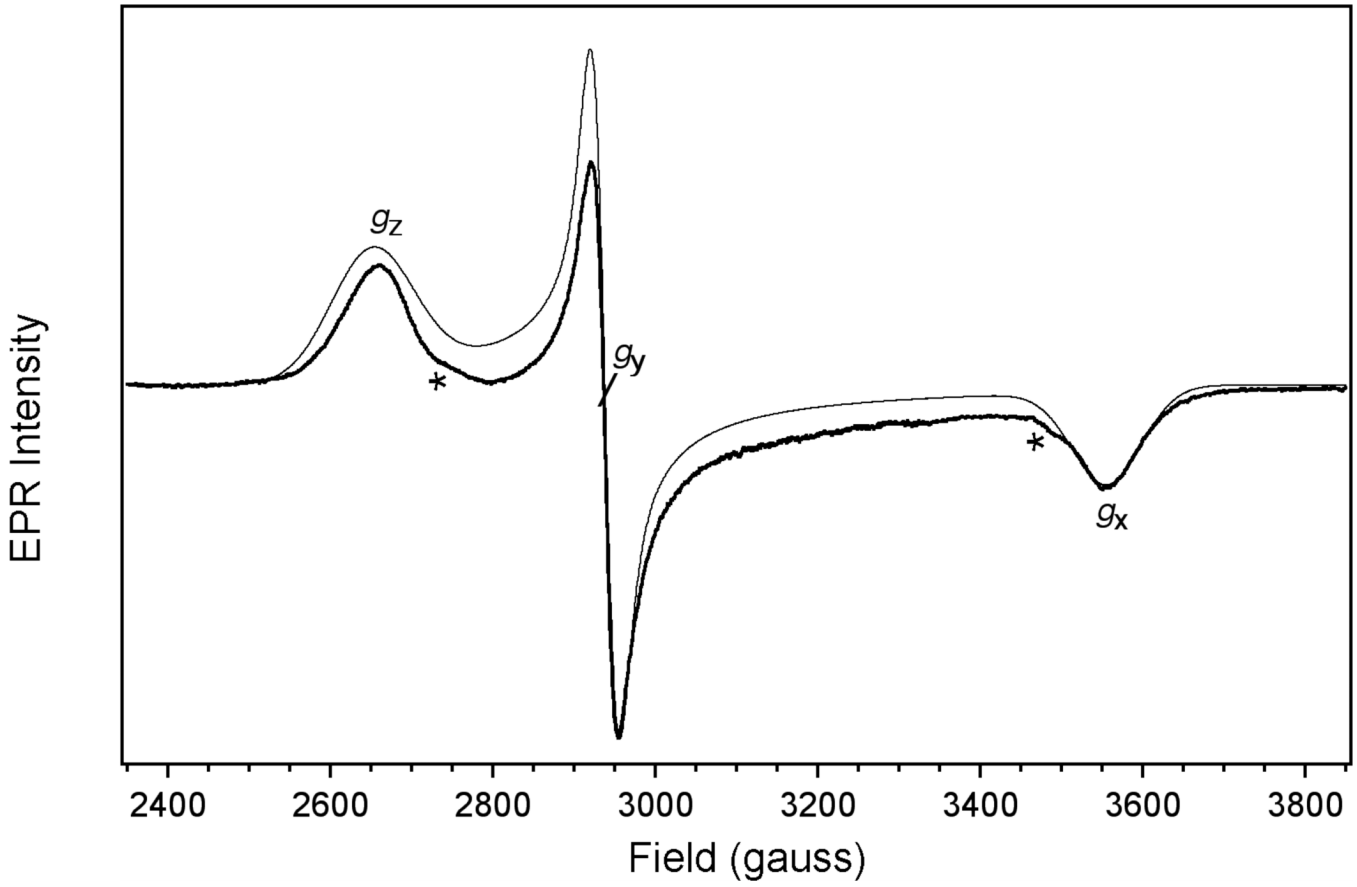

Figure 2.

X-band EPR spectrum of Fe(III)*Bx*RcoM-2 (thick line) and best-fit simulation (thin line). The sample was 250 μM heme in 50 mM borate buffer and 500 mM KCl, pH 8.0. The spectrum was recorded at 10 K, 9.3567 GHz microwave frequency, 0.505 mW microwave power, 3.2×10^5 receiver gain, 8.31 G modulation amplitude, 100 kHz modulation frequency and 163.84 ms time constant, using 10 added scans each containing 2048 data points. The background was corrected and the best-fit simulation was generated. *The unsimulated minor second signal, g_x and g_z components.

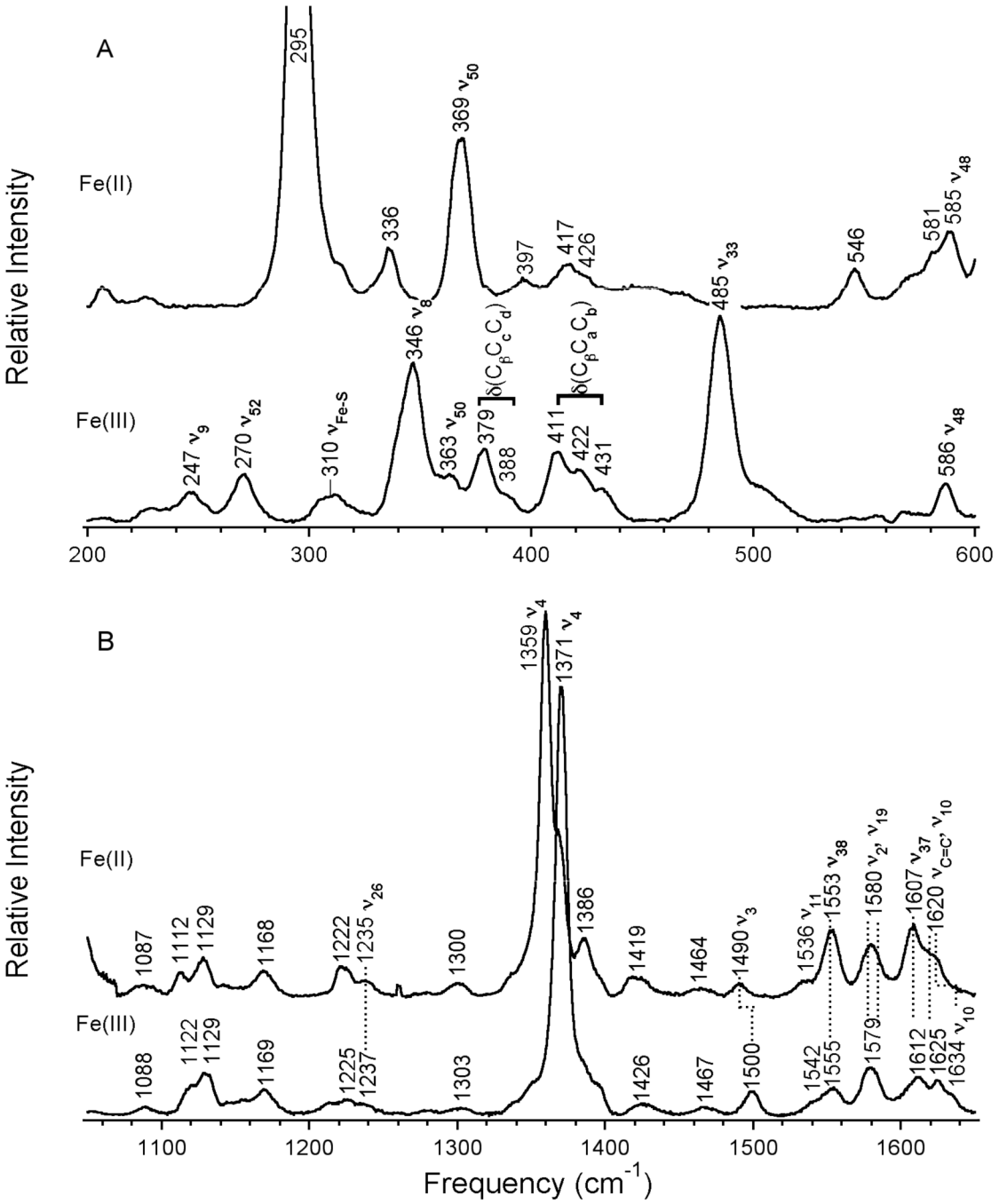

Figure 3.

Resonance Raman spectra of Fe(III)*Bx*RcoM-2 and Fe(II)*Bx*RcoM-2. The sample concentrations were 250 μM heme in 50 mM borate buffer and 500 mM KCl, pH 8.0. Reduction was performed using solid sodium dithionite. Spectra were acquired on the frozen samples at 77 K using the 413.1 nm Kr^+ laser line with ~50 mW power at the sample. Spectral windows are shown for **A)** 200−600 cm^{-1} and **B)** 1050−1650 cm^{-1} regions. Key vibrational modes are indicated.

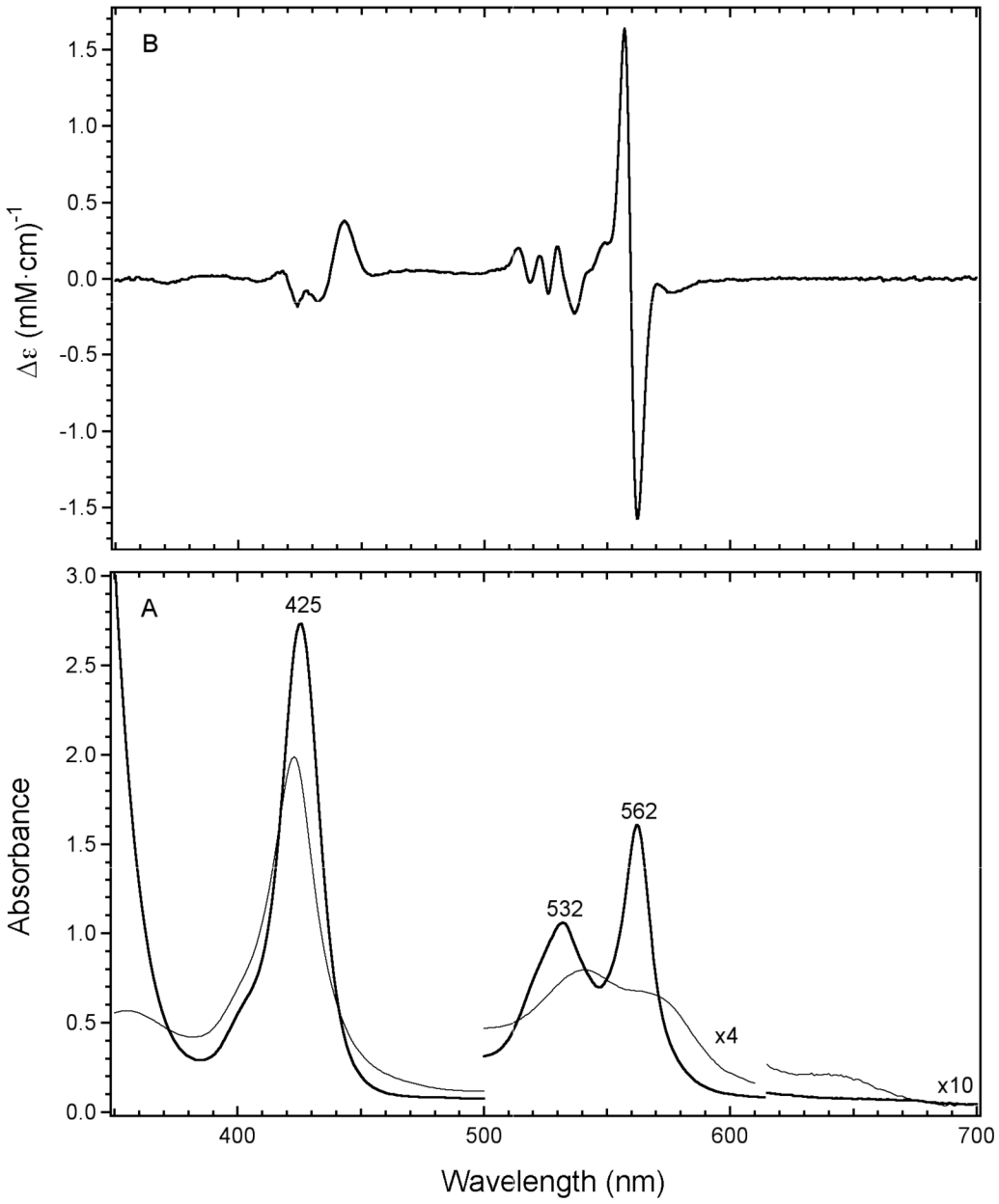

Figure 4.

Electronic absorption (A) and MCD (B) spectra of Fe(II)*Bx*RcoM-2. **A)** The electronic absorption sample was 12 μM heme in 25 mM EPPS buffer with 500 mM KCl, pH 8.0, at 25 °C. Sodium dithionite was added in slight excess as a solid to Fe(III)*Bx*RcoM-2 (thin line) to prepare Fe(II)*Bx*RcoM-2 (thick line). **B)** The MCD sample was approximately 30 μM heme in 25 mM EPPS buffer with 250 mM KCl, pH 8.0, ~55% glycerol. The average of 3 scans collected at 4.5 K under constant magnetic field (7 tesla) is shown.

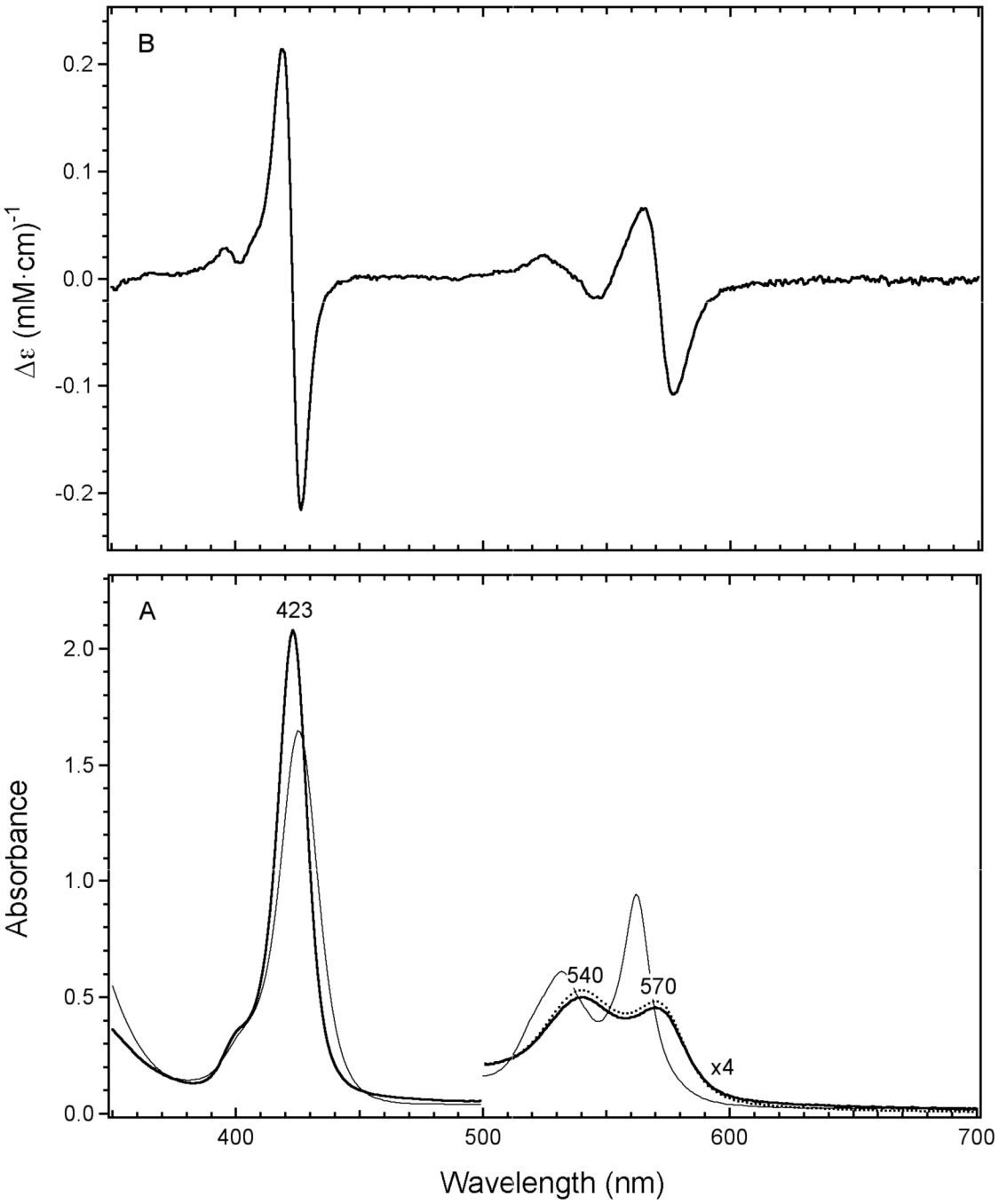

Figure 5.

Electronic absorption (A) and MCD (B) spectra of Fe(II)CO *Bx*RcoM-2. **A)** Electronic absorption spectra of Fe(II)CO *Bx*RcoM-2, with order of addition effects, are shown. A sample (~8 μM heme) with $CO_{(g)}$ present at time of reduction (solid line) is compared with a sample (~8 μm heme) with $CO_{(g)}$ injected after reduction (dashed line). The Fe(II) Soret is shown (thin line); the Fe(II)CO Soret is the same in both experiments. **B)** The MCD sample was ~30 μM heme in 25 mM EPPS buffer with 250 mM KCl, pH 8.0, ~55% glycerol. The average of 3 scans collected at 7 tesla and 100 K is shown. Samples were prepared in 25 mM EPPS buffer with 500 mM KCl, pH 8.0, maintained at 25 °C. Sodium dithionite solution was used to reduce

the protein samples in (A) and (B). For MCD (B), $CO_{(g)}$ was mixed with the Fe(III)*Bx*RcoM-2 sample before reduction.

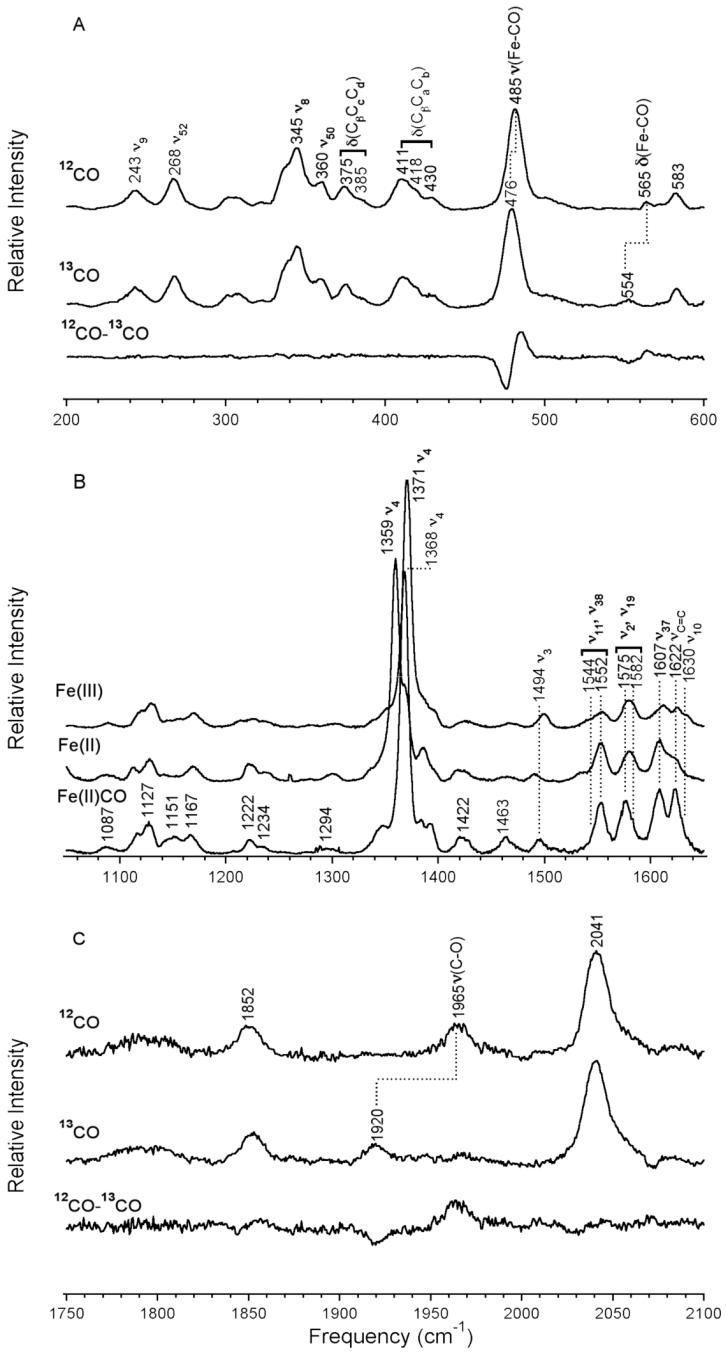

Figure 6.

Resonance Raman spectra for Fe(II)(^{12}CO) and Fe(II)(^{13}CO) *Bx*RcoM-2. The samples were 250 μM heme in 50 mM borate buffer and 500 mM KCl, pH 8.0. After $CO_{(g)}$ was injected into the Fe(III)*Bx*RcoM-2 sample headspace, reduction was performed using a sodium dithionite solution. Spectra were acquired on frozen samples at 77 K using the 413.1 nm Kr^+ laser line with ~7 10 mW power at the sample. The difference spectrum (^{12}CO-^{13}CO) is shown for the frequency ranges containing ν(Fe-CO), δ(Fe-CO) and ν(C-O). **A)** The lowest frequency window, 200−600 cm^{-1}, containing the stretching and bending modes ν(Fe-CO) and δ(Fe-CO). **B)** The mid-frequency window, 1050−1650 cm^{-1}, containing the major oxidation, spin and coordination state marker bands. Shown is a comparison of the Fe(III), Fe(II) and Fe(II)CO

states. **C)** The high frequency window, 1750−2100 cm^{-1}, containing the stretching mode ν(C-O). Key vibrational modes are indicated.

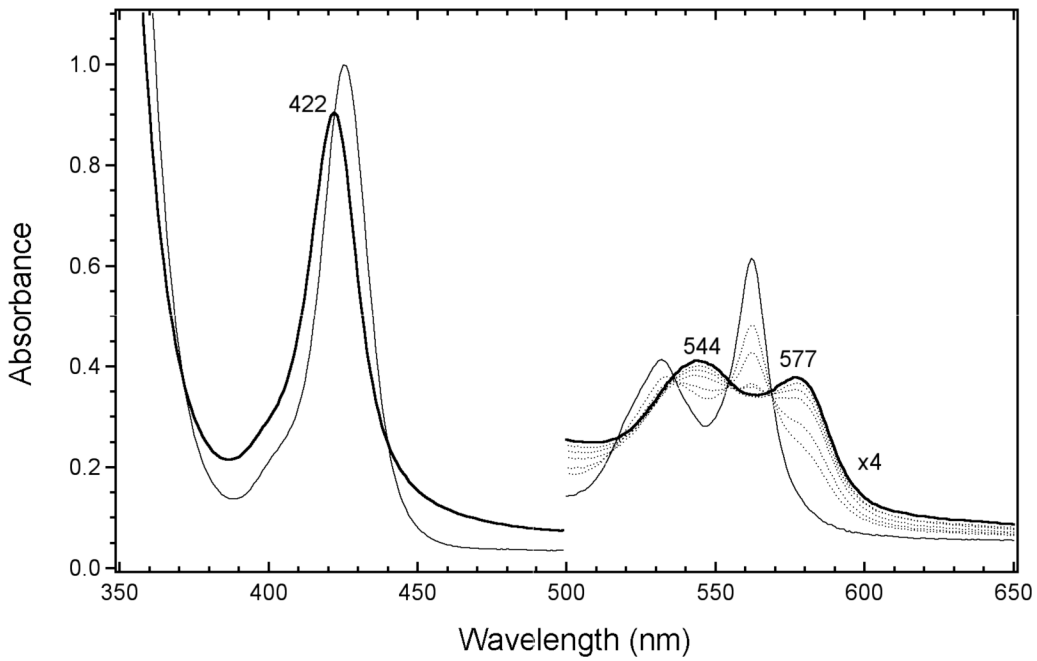

Figure 7.

Electronic absorption spectrum of Fe(II)NO *Bx*RcoM-2. The electronic absorption spectrum of Fe(II)NO *Bx*RcoM-2 (thick line) is shown overlaid on the Fe(II) spectrum (thin line). The conversion profile from the ferrous protein after a bolus of $NO_{(g)}$ was added is indicated in the α-β region (dotted). The sample was 6 μM heme in 25 mM EPPS buffer with 500 mM KCl, pH 8.0, maintained at 25 °C. The sample was prepared by reducing Fe(III)*Bx*RcoM-2 with solid sodium dithionite followed by addition of $NO_{(g)}$.

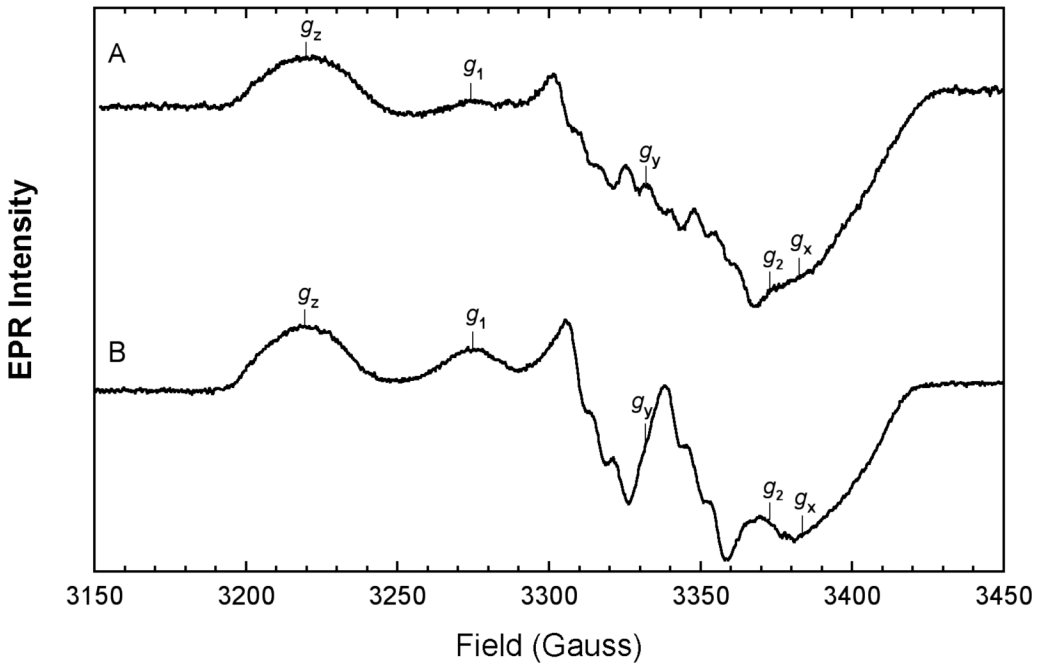

Figure 8.

X-band EPR spectra of **A)** Fe(II)(^{14}NO) and **B)** Fe(II)(^{15}NO) *Bx*RcoM-2. Each sample was approximately 200 μM heme in 50 mM borate buffer with 500 mM KCl, pH 8.0. The samples were prepared via reduction of Fe(III)*Bx*RcoM-2 followed by generation of $NO_{(g)}$. Spectra were recorded at 10 K, 9.3567 GHz microwave frequency, 0.16 mW microwave power, 6.3 × 10^5 receiver gain, 2.09 G modulation amplitude, 100 kHz modulation frequency, 163.84 ms time constant, using 10 added scans containing 2048 data points.

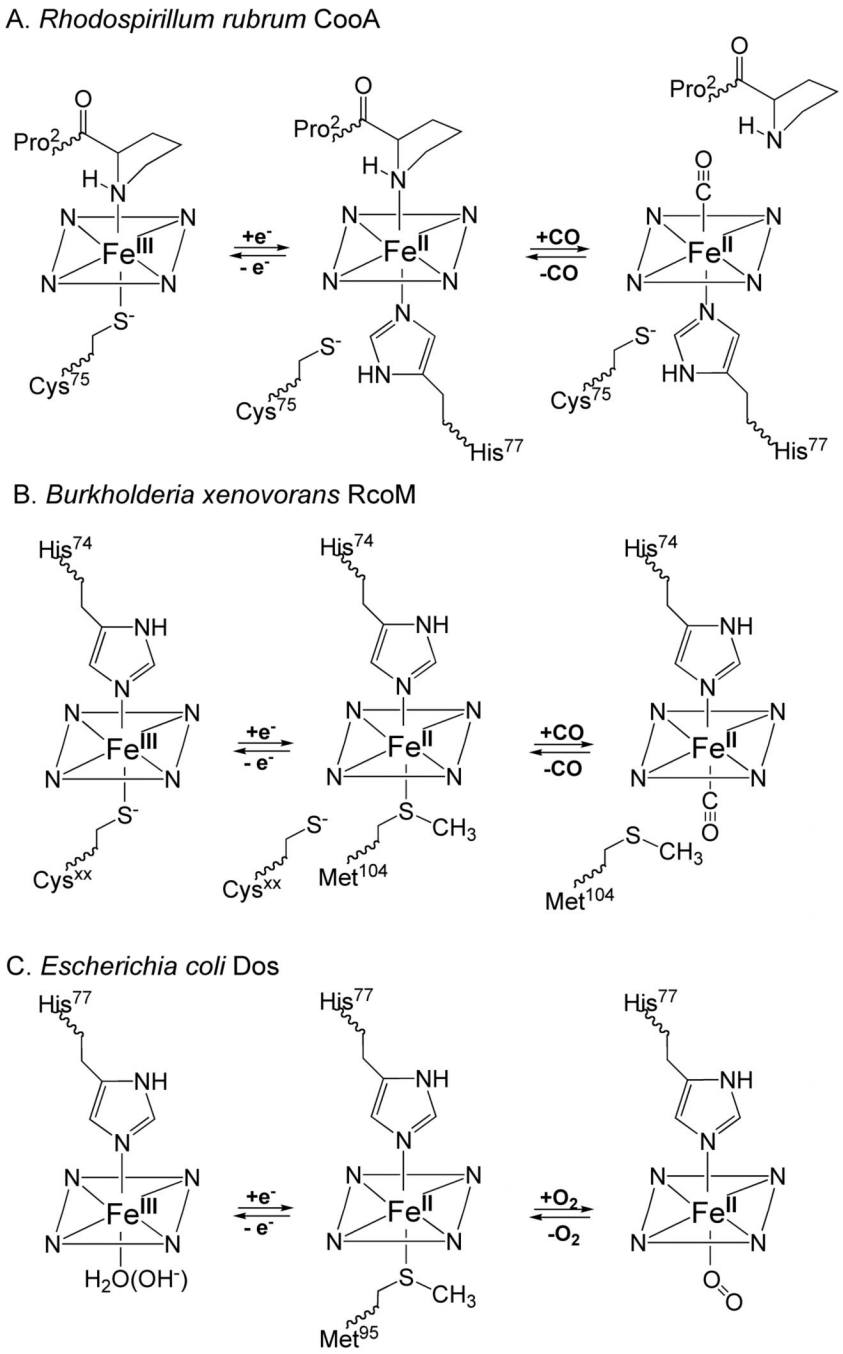

Scheme 1.

The heme coordination environments of: (A) *Rr*CooA (B) *Bx*RcoM and (C) *Ec*Dos. The essential features of the *Bx*RcoM redox and gas-binding mechanism (B) include: 1) a common histidine ligand in all states, 2) cysteine(thiolate) coordination to Fe(III), 3) methionine coordination to Fe(II), 4) selective replacement of methionine by CO.

Table 1

Comparison of electronic absorption peak positions for low-spin 6-coordinate Fe(III) heme proteins. The experimental values for *Bx*RcoM-2 are shaded.

Electronic Absorption							
Protein	**Ligands**	**δ**	**Soret**	**β**	**α**	**LMCT**	**Ref.**
***Bx*RcoM-2**	**?/Cys**	**354**	**423**	**541**	**565**	**640,730**	*a*
*Rr*CooA	Pro/Cys	362	424	540	574	649,750	(21)
$P450_{CAM}$+ImH	ImH/Cys	358	425	542	574	638,753	(72)
hCBS	His/Cys	365	428	550	NR	650,700	(56)
M80C cyt *c*	His/Cys	355	416	540	570	635,734	(72)
cytochrome *c*	His/Met		408	530	695		(73)
*Ec*Dos	His/H_2O		416	530	564		(74)
cytochrome b_5	His/His		413	532	566		(75)
neuroglobin	His/His		415	535	565		(59)

[a]This work.

Table 2

Comparison of EPR *g* values for selected Fe(III) heme proteins. The experimental values for *Bx*RcoM-2 are shaded.

EPR						
Protein	**Ligands**	**g_z**	**g_y**	**g_x**		**Ref.**
***Bx*RcoM-2**	**?/Cys**	**2.52**	**2.28**	**1.88**		*a*
*Rr*CooA	Pro/Cys	2.46	2.25	1.89	(major)	(37)
*Rr*CooA	Pro/Cys	2.58	2.25	1.84	(minor)	(37)
$P450_{CAM}$+ImH	ImH/Cys	2.56	2.27	1.87		(55)
hCBS	His/Cys	2.49	2.31	1.87	(major)	(56)
hCBS	His/Cys	2.43	2.31	1.90	(minor)	(56)
M80C cyt *c*	His/Cys	2.56	2.27	1.85		(57)
*Ec*Dos	His/H_2O	3.42	-	-		(76)
cytochrome b_5	His/His	3.03	2.23	1.43	pH 7.0	(77)
neuroglobin	His/His	3.14	2.16	1.34		(78)

[a]This work.

Table 3

Comparison of electronic absorption and MCD peak positions for selected 6-coordinate Fe(II) heme proteins. The experimental values for *Bx*RcoM-2 are shaded.

Electronic Absorption						
Protein	**Ligands**	**δ**	**Soret**	**β**	**α**	**Ref.**
***Bx*RcoM-2**	**?/?**		**425**	**532**	**562**	*a*
*Rr*CooA	His/Pro		425	529	559	(58)
hCBS (pH 9.0)	His/Cys		448	540	570	(56)
cytochrome *c*	His/Met		413	521	550	(79)
*Ec*Dos	His/Met		427	532	563	(4)
cytochrome b_5	His/His		423	526	556	(80)
neuroglobin	His/His		426	530	560	(59)

MCD		**Peak**	**Crossover**	**Peak**	**Peak**	**Crossover**	**Peak**	**Ref.**
***Bx*RcoM-2**	**?/?**	**417**	**421**	**424**	**557**	**560**	**562**	*a*
*Rr*CooA	His/Pro	416[b]	420	425[b]	550[b]	554	558[b]	(81)
hCBS (pH 9)	His/Cys	445[b]	448	452[b]	563[b]	566	569[b]	(56)
cytochrome *c*	His/Met	414	420	425	544[b]	546	549[b]	(82)
*Ec*Dos	His/Met	NR[c]	NR[c]	430	558	561	565	(74)
cytochrome b_5	His/His	415	426	438	544	547	549	(82)

[a] This work.

[b] Peak positions were not reported in the original paper and are presented from inspection of the data.

[c] Not reported.